Materials Today Energy 7 (2018) 169–189

Contents lists available at ScienceDirect

Materials Today Energy

journal homepage: www.journals.elsevier.com/materials-today-energy/

Advances and challenges to the commercialization of organic–inorganic halide perovskite solar cell technology

Longbin Qiu [1], Luis K. Ono [1], Yabing Qi*

Energy Materials and Surface Sciences Unit (EMSS), Okinawa Institute of Science and Technology Graduate University (OIST), 1919-1 Tancha, Onna-son, Kunigami-gun, Okinawa 904-0495, Japan

ARTICLE INFO

Article history:
Received 25 May 2017
Received in revised form
1 September 2017
Accepted 10 September 2017
Available online 21 September 2017

Keywords:
Perovskite solar cell
Large scale
Lifetime
Cost-performance analysis
Toxicity

ABSTRACT

When transferring photovoltaic technologies from laboratory-scale fabrication to industrial applications, low cost, large area, high throughput, high solar-to-energy power conversion efficiency, long lifetime, and low toxicity are crucial attributes. In recent years, organic–inorganic halide perovskite solar cells have emerged as a promising high-performance, cost-effective solar cell technology. However, most of the best reported efficiencies have been obtained on small active-area devices (~0.1 cm^2). Therefore, development of protocols to industrialize such a technology is of paramount importance. In this article, we review the progress of perovskite solar cells with a particular emphasis on fabrication processes and instrumentation that have scale-up potential. For successful commercialization, the capacity to fabricate large-area modules is essential. Long-term stability is discussed, focusing on lifetime measurement and quantification protocols for commercialization. Cost-performance and life-cycle assessment analysis based on recently reported state-of-the-art perovskite solar cells are discussed. These analyses offer insights regarding required efficiency, module area size, and lifetime, in order for perovskite solar cells to be competitive with existing photovoltaic technologies. Finally, lead toxicity and possible solutions to this issue will be discussed. In the outlook, we outline future research directions based on reported results and trends in the field.

1. Introduction

Development of technologies to transform renewable energy into electricity is essential to societal advancement. To harvest solar energy, various photovoltaic techniques have been invented and developed in the past half century. So far, the most widely commercialized solar cells include crystalline silicon solar cells (69.5%), multicrystalline silicon solar cells (23.9%) and CdTe solar cells (6.6%), as of 2015 [1]. Certified power conversion efficiencies (PCE) of these solar modules are as high as 24.4% for single crystalline silicon, 19.9% for multicrystalline silicon, and 18.6% for CdTe, respectively [2]. For commercialized solar modules, PCE is only ~2% lower than the certified highest PCE. However, due to the high fabrication costs of these photovoltaic technologies, the total solar energy that they can harvest amounts to only ~1% of the world's current energy consumption [3]. To make full use of available solar energy, we must either reduce the cost of existing solar cell technology or develop new photovoltaic technologies.

Perovskite solar cells, the most promising new technology in academia and industry, has promise as a highly competitive alternative to silicon solar cells and other commercial alternatives. Perovskite solar cells are high-performance photovoltaic devices which have the potential to enter the market in the near future. Low processing costs and highly abundant raw materials may permit a short energy payback time and low overall CO_2 emissions. After an impressive increase in PCE from ~10% in 2012 to ≤22.1% in early 2016, experts expect to see further improvements in efficiency in the next several years [4–6]. Perovskite solar cell research is still in its infancy considering that the first work was only published in 2009 [7]. So far, there are a few companies focusing on development of perovskite solar panel products: Microquanta Semiconductor, Solar-Tectic, Oxford Photovoltaics, Saule Technologies, and Dyesol [8].

To commercialize perovskite solar cell technology in the near future, there are several fundamental issues that need to be addressed: (i) controllable thin film growth and deposition, (ii)

* Corresponding author.
E-mail address: Yabing.Qi@OIST.jp (Y. Qi).
[1] These authors contributed equally to this work.

http://dx.doi.org/10.1016/j.mtener.2017.09.008
2468-6069/

scalable and reproducible process, (iii) high stability and long lifetime, and (iv) low toxicity. To be competitive, manufacturing companies will be also concerned about cost. Although the raw materials for making perovskite solar cells are inexpensive and abundant, recent analyses of cost-performance and commercialization requirements are not entirely positive [9–11]. To make perovskite solar cells competitive, several goals need to be reached. For example, the levelized cost of electricity (LCOE) for residential use is 9.0 cents per kWh by 2020, and is expected to decline to 5.0 cents/kWh by 2030 [1]. This is a huge challenge for perovskite technology at present.

The LCOE is an important standard for comparing different photovoltaic technologies. It is also a key consideration for customers installing solar panels. Calculation of the LCOE includes the total cost and energy output. The cost depends upon raw materials, installation, maintenance, fabrication, and transportation costs, while energy output depends on the efficiency and lifetime of solar modules. In a recent report, Chang et al. claimed that even if the raw material cost is zero, to reach 9.0 cents/kWh by 2020 will require a PCE >20% and a lifetime >20 years (1 m × 1 m panel) [12]. Concerted effort will be required to improve the PCE and lifetime of large perovskite solar panels.

The rapid increase in PCE for perovskite solar cells is impressive, being several times faster than any other solar technology. However, in most cases these high efficiencies were obtained on lab-scale cells with very small areas (~0.1 cm^2). The first issue to emphasize is the need to develop fabrication methods that enable high performance on large perovskite solar panels [13,14]. Thus far, the reported largest perovskite solar cell module had a total area of 100 cm^2 with a module maximum power of 429.7 mW (PCE of 4.3%) [15]. For a certified module with an area of 36 cm^2, a PCE of 12.1% was demonstrated [2]. In general, performance of large-area perovskite solar modules depends on whether the perovskite deposition technique enables controlled growth and deposition of high-quality perovskite thin films over large areas. The second issue concerns the lifetime of these large-scale perovskite solar cells. At present, stability is still a severe limitation and many perovskite cells survive only several months. However, a lifetime of ≥20 years is required to achieve a sufficiently low LCOE. Mechanisms of degradation and possible solutions to the stability issue are under intensive investigation by research groups worldwide. The third issue that is a significant concern to investors, fabricators, and customers is the toxicity of lead, which presents a huge pollution source in manufacturing and disposal phases. The large amount of lead in a perovskite solar farm could potentially cause serious damage to the environment and to humans.

In this review, we summarize recently developed perovskite film deposition techniques and evaluate their suitability for industrial production of perovskite solar cells and modules. Our discussion of stability and device lifetime focuses mainly on measurement standards and issues relative to commercialization. Thereafter, we present a cost-performance analysis for perovskite technology and the required efficiency, scale, and lifetime for such solar cells to compete with existing photovoltaic technologies. Finally, the toxicity of lead and possible solutions to this issue will be reviewed.

2. Fabrication methods aiming at scale-up

To fabricate large-area perovskite films of high quality (good film uniformity, reduced surface roughness, low density of structural defects, such as pinholes, etc.), various thin-film deposition technologies have been developed, including spin-coating, optimized for large areas [16–18], doctor blading [15], slot-die coating [19], printing [20], spray-deposition [21], soft-cover deposition [22], dip coating [23], and vapor-based deposition [24,25]. For industrial applications, the second step is to fabricate solar modules, and the third step is to integrate multiple solar modules into solar panels. Large-area modules and panels have been designed and fabricated for perovskite solar cells (Fig. 1). However, for commercial fabrication, we should ask the following questions: Are these techniques promising for high-throughput deposition of perovskite layers? Are these techniques reproducible? What perovskite film formation mechanisms do these deposition techniques entail? What parameters determine the quality (e.g., film crystallinity, morphology, etc.) of perovskite films deposited by these techniques? Is it possible to reduce the number of process steps in these deposition techniques?

For large area devices and modules, transparent conductive electrodes (TCO) must be considered in terms of both sheet resistance and cost. Due to the sheet resistance of the TCO, the fill factor will decrease significantly when the active area of a single solar cell device exceeds a certain threshold [27]. Wired transparent electrodes were developed [28] to overcome the high resistance of transparent electrodes and greatly assisted fabrication of large-area solar cells. Combining wired transparent electrodes with spin coating, a perovskite solar cell of 25 cm^2 was fabricated with an efficiency of 6.8%. This is the largest single perovskite solar cell reported so far. On the other hand, the commonly used FTO glass substrate is the most expensive part of perovskite solar cells [29,30]. Less often, ITO glass substrates have been used in perovskite solar cells. So far there is no alternative to FTO/ITO for perovskite solar cell substrates. Development of a large-crystal, perovskite layer could make metal grid electrodes possible. In this section, we focus mainly on perovskite deposition techniques and their influence on perovskite film qualities, followed by a discussion of large-scale solar cells and modules fabricated using these techniques. Table 1 summarizes the performance of perovskite solar cells/modules with active areas larger than 1 cm^2.

2.1. Spin coating

Spin coating is widely used to deposit small-area thin films in research laboratories. Although this technique might not be suitable for large-area, high-throughput film deposition, it can be conveniently used to optimize ink formulations in fundamental studies in which cell area is not major objective. Typically, in spin coating, a small amount of solution is first dropped onto a substrate to fully wet the substrate surface (Fig. 2a). Subsequently, the substrate is fully covered with a layer of solution and spun to accelerate evaporation of the solvent [31]. The film thickness is controlled by the concentration of the solution and rotational velocity. The volatility of solvents affects the perovskite crystallization process [31]. In general, with conventional spin coating, a one-step process with PbI_2/MAI or $PbCl_2$/MAI as precursors and γ-Butyrolactone (GBL), Dimethylformamide (DMF) or Dimethyl sulfoxide (DMSO) as solvent leads to poor film quality [32,33]. Even though all processing conditions (annealing temperature, solution concentration and spinning speed) have been considered, spin-coated perovskite film quality is often poor, with a high density of pinholes and small grain sizes. These pinholes cause shunt pathways that degrade solar cell performance. With additives engineering the crystallization of perovskite could be finely tuned and perovskite films with significantly improved quality can be prepared for high performance solar cells [34,35]. For example, by using lead acetate as lead source the perovskite crystal growth is much faster. Ultrasmooth and pinhole-free perovskite films were demonstrated by a simple one-step coating process [36]. Another recent work also reported that by using methylammonium acetate and thio-semicarbazide as additives, it was possible to form a highly uniform perovskite film

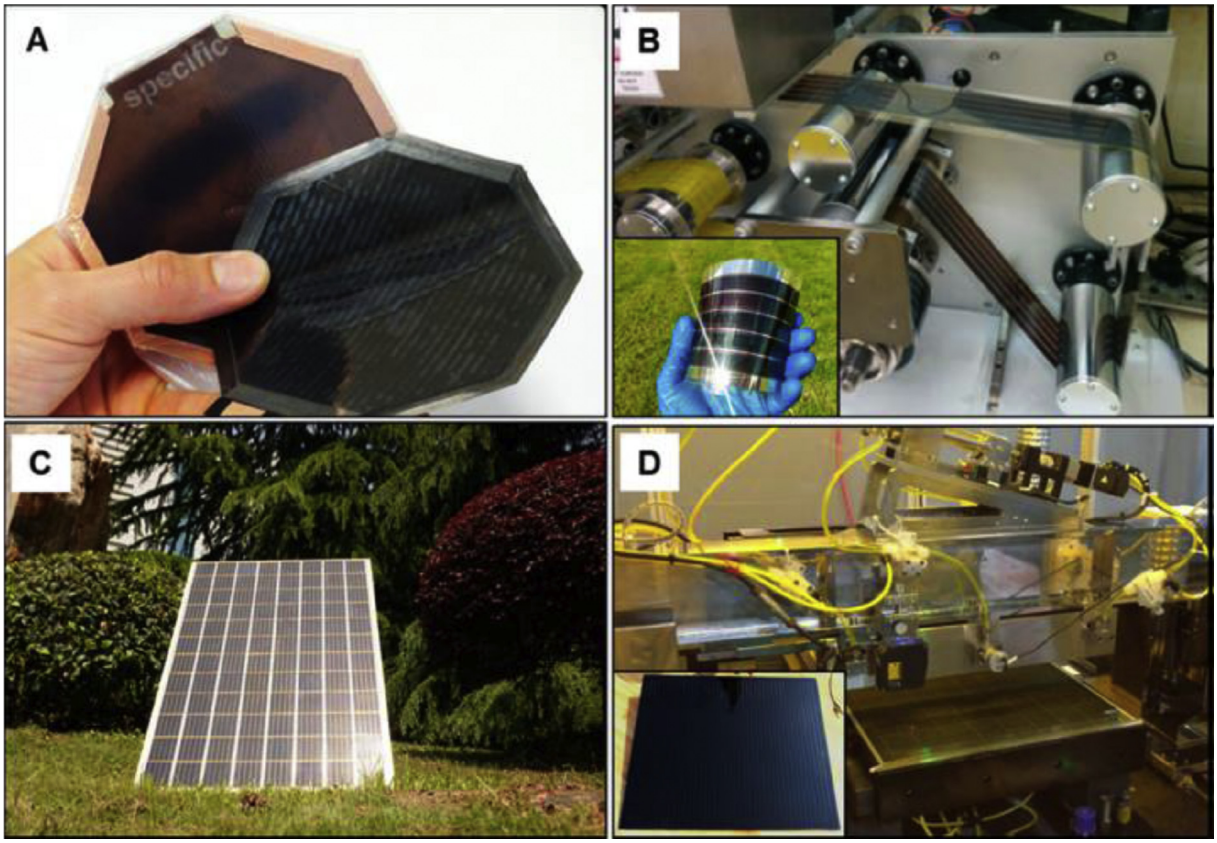

Fig. 1. Large area perovskite solar cell modules and panels. **a.** Printed perovskite solar cells on low-cost metal foil. **b.** Roll-to-roll fabrication of $MAPbI_3$ perovskite thin films. **c.** Carbon-based, hole-conductor-free mesoscopic perovskite solar panel. **d.** Slot-die coating the perovskite thin film on a rigid substrate. Reprinted with permission from Ref. [26]. Copyright (2016) American Chemical Society.

with full coverage and large crystal size through a simple one-step spin coating process. A certified efficiency of 19.19% was obtained for devices with an area of 1.025 cm^2 [37]. A two-step sequential deposition process, developed to deposit high coverage perovskite films [38], complicates control over the conversion rate of PbI_2 to perovskite.

Recently, it has been shown that formation of a PbI_2-DMSO-MAI intermediate significantly enhances film coverage and quality using an advanced anti-solvent engineering method [39–41]. When performed in a moderately humid environment, the subsequent annealing process further enhances thin film quality [42]. With development of the anti-solvent process, the two-step interfusion process [43,44], and the solvent annealing process [45,46], high-quality, full-coverage perovskite films have been produced with a higher level of reproducibility (Fig. 3a). Other innovative processes, such as drying with N_2 gas [47] and vacuum flash drying [48] were also developed and able to deposit high-quality films (Fig. 3b–c). A preheated hot substrate could accelerate crystallization eliminating the anti-solvent process and post-treatment. Without prolonged annealing, it would be easier to control the composition of the film, which is expected to conform to the precursor solution composition [49]. In addition, this hot-casting process could be transferred to a much simpler dip-coating process for large area film deposition. Both high performance and large-area scalability of perovskite solar cells are closely related to perovskite film quality.

Spin coating can be used to fabricate intermediate-area perovskite solar cells and modules. The most popular deposition technique for intermediate-area perovskite solar cell devices is spin coating (Table 1). With a modified interface layer, a 1-cm^2 perovskite solar cell was first fabricated with a certified efficiency of 15.6% [52]. With an improved gradient heterojunction structure for charge separation/transport, performance increased to 18.21% [53]. Recently a vacuum, flash–assisted process has been developed for solution-processed large-area devices [48]. A solar cell with a 1-cm^2 area produced by this technique showed a maximum efficiency of 20.5% and a certified efficiency of 19.6% (Fig. 3c). Modules of perovskite solar cells fabricated using spin coating achieved areas up to 100 cm^2 (active area of 60 cm^2) with a PCE of 8.7% [54].

However, spin coating is not compatible with high-throughput, large-area solar cell fabrication. Spin-coated films are not uniform from center to edge [55]. Also, during the spin coating, a large amount of solution containing raw materials and solvents is wasted, increasing costs. When enlarging solar cell area using spin coating, performance generally decreases significantly compared with small-area devices [56,57]. The reduced performance is caused by an increase in series resistance and decreased film quality. Thus, scaling-up perovskite solar cell fabrication using spin coating faces challenges of both performance and cost. Nevertheless, studies on perovskite solar cells prepared by spin coating can provide valuable insights into properties of precursor solutions and mechanisms to form solid films from wet films. This step is important before a solution process is transferred to industrial-scale. Recently it was reported that a precursor solution with a suitable ratio of MACl could significantly facilitate high-quality film deposition with large grain sizes. This solution is suitable for both spin coating and other large-area deposition techniques, such as doctor blading [58,59].

Table 1
Perovskite solar cells with active areas larger than 1 cm^2.

Solar cell architecture[a]	Perovskite fabrication method	Cell structure	Electrode active area (cm^2)	PCE (%)	Jsc (mA/cm^2)	Voc (V)	FF	Ref.
FTO/c-TiO_2/mp-TiO_2/$FA_{0.81}MA_{0.15}PbI_{2.51}Br_{0.45}$/Spiro-MeOTAD/Au	Spin-coating	Single cell	1	20.18	23.95	1.147	0.748	[48]
FTO/c-TiO_2/$Cs_{0.05}FA_{0.8}MA_{0.15}PbI_{2.55}Br_{0.45}$/spiro-MeOTAD/Au	Spin-coating	Single cell	1.1	19.5	21.5	1.195	0.757	[90]
FTO/$Li_{0.05}Mg_{0.15}Ni_{0.8}O$/$MAPbI_3$:PCBM/PCBM/$Ti_{0.95}Nb_{0.05}Ox$/Ag	Spin-coating	Single cell	1.02	18.75	21.98	1.08	0.79	[53]
FTO/$Li_{0.05}Mg_{0.15}Ni_{0.8}O$/$MAPbI_3$/PCBM/$Ti_{0.95}Nb_{0.05}Ox$/Ag	Spin-coating	Single cell	1.02	16.2	20.21	1.07	0.748	[52]
ITO/NiOx/$MAPbI_3$/PCBM/MAcac/Ag	Spin coating	Single cell	1.01	16.05	21.21	1.057	0.716	[91]
FTO/c-TiO_2/$MAPbI_3$/spiro-MeOTAD/Au	Spin-coating	Single cell	1	11.70	17.62	1.09	0.61	[92]
FTO/c-TiO_2/$MAPbI_3$/spiro-MeOTAD/Au	Spin-coating	Single cell	1	12.6	19.6	0.96	0.671	[93]
ITO/PEIE/PCBM/$MAPbI_3$/P3HT/Au	Spin-coating	Single cell	1	13.45	22.25	0.904	0.669	[94]
ITO/c-TiO_2/$MAPbI_3$:PAN/Spiro-MeOTAD/Ag	Spin-coating	Single cell	1	7.32	14.28	0.99	0.517	[17]
FTO/c-TiO_2/mp-TiO_2/$MAPbI_3$/Spiro-MeOTAD/Au	Spin-coating	Single cell	1	14.5	19.6	1.07	0.69	[95]
FTO/NiO_x/$MAPbI_{3-x}Cl_x$/PCBM:PEI/Ag	Spin-coating	Single cell	1	15.4	21.0	1.06	0.691	[49]
		Module	25	12.0	2.60	7.98	0.582	
FTO/c-TiO_2/mp-TiO_2/$MAPbI_3$/Spiro-MeOTAD/Au	Spin-coating	Single cell	1.05	13.55	20.13	0.984	0.684	[96]
FTO/c-TiO_2/$FA_{0.1}MA_{0.9}PbI_3$/spiro-MeOTAD/Au	Spin-coating	Single cell	1.1275	17.05	22.56	1.12	0.678	[57]
FTO/c-TiO_2/$MAPbI_3$/spiro-MeOTAD/Ag	Spin-coating	Single cell	1.2	16.3	21.9	1.10	0.677	[56]
ITO/PEDOT:PSS/$MAPbI_3$/PC71BM/Ca/Al	Spin-coating	Single cell	1.3	16.7	22.51	0.99	16.7	[97]
		Module	11.25	15.4	4.25	4.69	15.4	
ITO/PEDOT:PSS/$MAPbI_3$/PCBM/BCP/Al	Spin-spray coating	Single cell	1.5	6.06	18.2	0.98	0.34	[98]
ITO/Al grid/PEDOT:PSS/$MAPbI_3$/PCBM/LiF/Ag	Spin-coating	Single cell	25	6.8	13.1	0.92	0.56	[28]
FTO/c-TiO_2/mp-TiO_2/$MAPbI_3$/spiro-MeOTAD/Au	Spin-coating	Single cell	3.36	5.9	10.09	0.91	0.651	[99]
		Module	16.8	5.1	1.96	4.31	0.603	
FTO/c-TiO_2/mp-TiO_2/$MAPbI_3$/P3HT/Au		Single cell	3.36	6.3	12.2	0.909	0.564	
		Module	16.8	5.1	2.19	4.45	0.526	
FTO/c-TiO_2/mp-TiO_2/$MAPbI_3$/spiro-MeOTAD/Au	Spin-coating	Module	10.08	13.0	4.66	4.21	0.665	[100]
ITO/c-TiO_2/$MAPbI_{3-x}Cl_x$/spiro/Au	Spin-coating	Module	4	13.6	19.9	0.91	0.75	[101]
ITO/PEDOT:PSS/$CH_3NH_3PbI_{3-x-y}Br_xCl_y$/PCBM/Ca/Al	Spin-coating	Module	25.2	14.3	2.12	9.05	0.744	[18]
FTO/c-TiO_2/mp-TiO_2/Graphene/$MAPbI_3$/Spiro-MeOTAD/Au	Spin-coating	Module	50.6	12.6	2.27	8.57	0.646	[102]
ITO/PEDOT:PSS/$MAPbI_3$/PCBM/LiF/Ag	Spin-coating	Module	60	8.7	1.9	8.1	0.57	[54]
ITO/PEDOT:PSS/$MAPbI_3$/PCBM/Au	Spin-coating	Module	40	12.9	2.02	10.1	0.637	[103]
		Single cell	0.096	18.1	20.9	1.1	0.79	
FTO/Au-busbar/c-TiO_2/PCBM/$MAPbI_3$/spiro-MeOTAD/Au	Spin-coating	Single cell	1.2	17.33	21.38	1.111	0.729	[58]
	Doctor blading	Single cell	1.2	15.30	21.47	1.068	0.668	
		Module	11.09	14.06	/	4.396	/	
FTO/c-TiO_2/mp-TiO_2/$MAPbI_3$/P3HT/Au	Doctor blading	Single cell	0.1	13.3	18.9	1.0	0.705	[15]
		Module	10.1	10.4	17.17	4.11	0.581	
		Module	100	4.3	7.48	9.61	0.538	
ITO/PEDOT:PSS/$MAPbI_{3-x}Cl_x$/C60/Al	Doctor blading	Single cell	1.01	7.32	12.47	0.854	0.687	[73]
FTO/NiO/$MAPbI_3$/PCBM/BCP/Ag	Soft-cover deposition	Single cell	1	17.6	1.02	21.8	0.787	[22]
FTO/c-TiO_2/mp-ZrO_2+MA(AVA-I)PbI_3/Carbon	Screen printing	Module	31	10.46	19.6	3.72	0.575	[20]
		Module	70	10.75	17.72	9.63	0.629	
FTO/c-TiO_2/$MAPbI_3$/spiro-MeOTAD/Au	Spray coating	Single cell	1	13.09	18.59	1.032	0.682	[50]
FTO/c-TiO_2/mp-TiO_2/$MAPbI_3$/Spiro-MeOTAD/Au	Spray coating	Single cell	1	13.0	19	0.99	0.69	[67]
FTO/c-TiO_2/$MAPbI_{3-x}Cl_x$/PTAA/Au	Spray coating	Module	40	15.5	2.10	10.5	0.7016	[68]
PET/ITO/ZnO/$MAPbI_3$/P3HT/Ag	Slot-die coating	Module	40	0.93	1.35	2.75	0.25	[19]
FTO/c-TiO_2/$MAPbI_{3-x}Cl_x$/spiro-MeOTAD/Au	Vacuum sequential deposition	Single cell	1	13.84	20.77	0.98	0.68	[104]
ITO/PEDOT:PSS/polyTPD/$MAPbI_3$/PCBM/Au	Vacuum co-evaporation	Single cell	0.98	8.27	14.76	1.05	0.52	[105]
FTO/c-TiO_2/$HC(NH_2)_2PbI_{3-x}Cl_x$/spiro-MeOTAD/Au	CVD	Single cell	1	7.7	18.4	0.97	0.43	[106]
FTO/c-TiO_2/mp-TiO_2/$MAPbI_3$/spiro-MeOTAD/Au	Low pressure CVD	Single cell	1	8.35	14.79	0.97	0.538	[107]
		module	8.4	6.22	3.43	2.93	0.62	
FTO/c-TiO_2/$HC(NH_2)_2PbI_{3-x}Cl_x$/spiro-MeOTAD/Au	CVD	Single cell	2	10.4	19.5	1.02	0.53	[25]
		Single cell	8.8	9.5	16.9	0.98	0.57	
		Single cell	12	9	17.8	0.94	0.54	

[a] Abbreviations: ITO = indium tin oxide; FTO = fluorine doped tin oxide; c-TiO_2 = compact layered TiO_2; mp-TiO_2 = mesoporous layered TiO_2; spiro-MeOTAD = 2,7′−7,7′-tetrakis-(*N*,*N*-di-*p*-methoxyphenylamine)-9,9′-spirobifluorene; PCBM = [6,6]-phenyl-C60,61 butyric acid methyl ester; MAcac = metal (Ti, Zr, Hf) acetylacetonate; PTAA = Poly[bis(4-phenyl)(2,4,6-trimethylphenyl)amine]; PEDOT:PSS = poly(3,4-ethylenedioxythiophene):poly(styrenesulfonate); P3HT = Poly(3-hexylthiophene-2,5-diyl) region regular; PAN = polymer polyacrylonitrile; PEI = polyethylenimine; BCP = bathocuproine; polyTPD = poly(*N*,*N*′-bis(4-butylphenyl)-*N*,*N*′-bis(phenyl)benzidine); AVA-I = 5-aminovaleric acid reacted with hydriodic acid in equimolar ratio.

To develop large-scale perovskite solar cell production, researchers have applied various existing technologies (e.g. coating technologies developed for fabricating organic solar cells) as well as novel methods. Examples of large-scale continuous perovskite film deposition processes that can be integrated into roll-to-roll continuous solution processing, include spray coating, slot die coating, screen printing, and doctor blading. Perovskite films can also be deposited using dry deposition processes, such as vacuum evaporation, chemical vapor deposition, etc.

2.2. Spray coating

Spray coating has been widely employed to deposit perovskite films and compact TiO_2 films and is compatible with large-scale, high-throughput fabrication (Fig. 2b). The first attempt to prepare perovskite films using spray coating borrowed the method from polymer solar cell fabrication [21]. An ultrasonic spray coating technique was explored to deposit perovskite thin films in ambient conditions. With a mono-solvent system of DMF or DMSO and

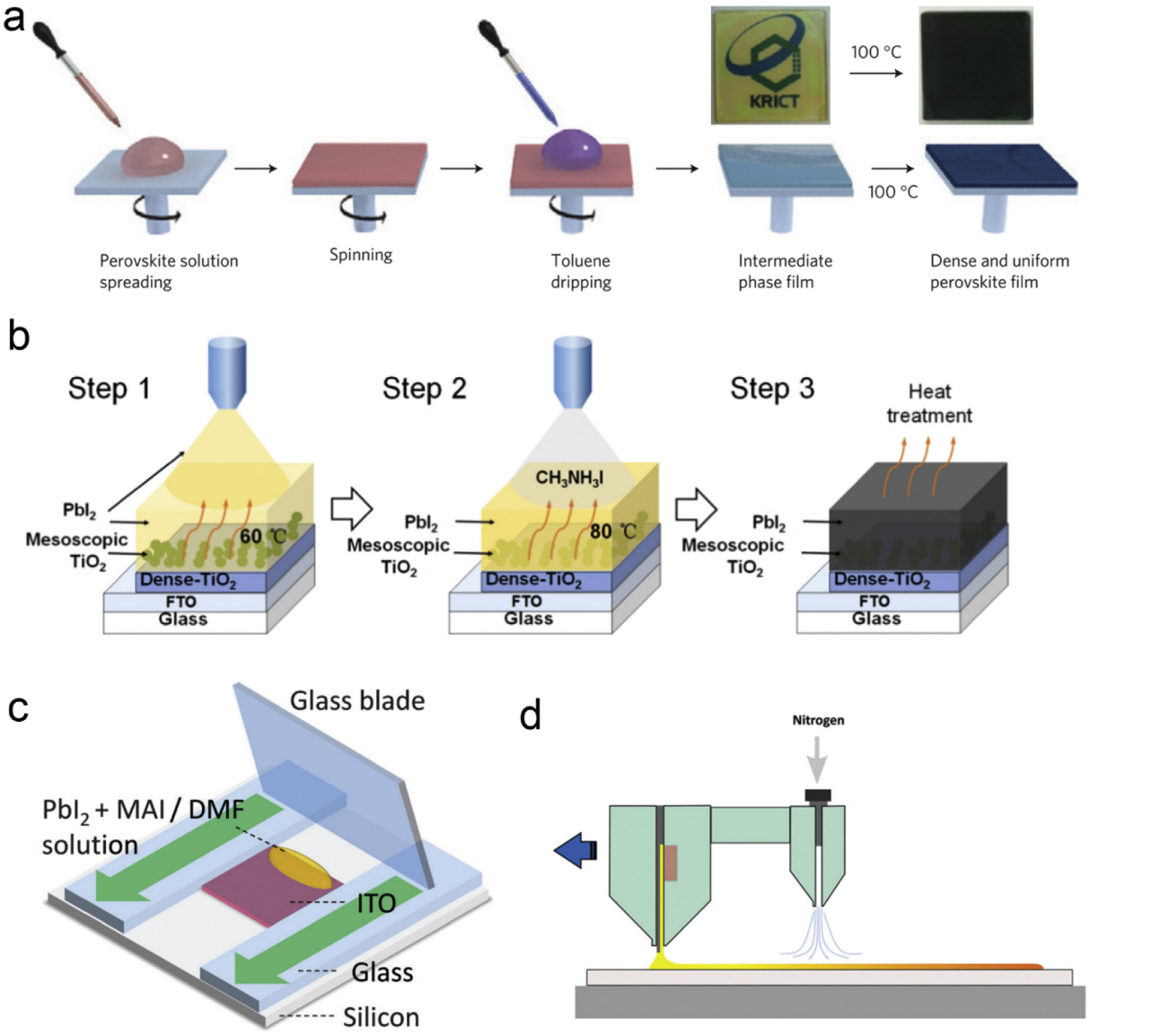

Fig. 2. Scalable techniques for large area perovskite film deposition. **a.** Spin coating. Reproduced with permission [40]. Copyright 2014, Nature Publishing Group. **b.** Spray coating. Reproduced with permission [50]. Copyright 2016, Elsevier. **c.** Doctor blade coating. Reproduced with permission [51]. Copyright 2013, The Royal Society of Chemistry. **d.** Slot die coating. Reproduced with permission [19]. Copyright 2015, John Wiley and Sons.

$PbCl_2$ and MAI as solutes, the deposition parameter space was investigated to achieve higher coverage of perovskite films [21]. Film drying time, substrate temperature, solvent volatility, and post annealing conditions are parameters in spray coating that require precise control to form high-coverage perovskite film. An inverted-structure champion cell with an 11% PCE and an active area of 0.025 cm^2 was realized, indicating the potential of spray coating in fabricating perovskite solar cells [21]. A similar optimization process was performed in a normal-structure device with TiO_2 as the bottom layer and the champion cell PCE of 13% (0.065 cm^2 active area) was obtained on a glass/ITO substrate [60]. On low-temperature processed TiO_2 deposited on a PET/ITO substrate, an efficiency of 8.1% was attained on a flexible device, which is comparable with roll-to-roll processing [60]. A simpler device employing a hole transport layer-free structure and a spray coated $MAPbI_3$ film with a thickness of 3.4 μm also showed an efficiency of 6.9% [61].

This spray coating process is suitable for various perovskite precursor solutions including PbI_2, MAI [62], CsI [63], FAI [64] solution for two-step spray-assisted solution processes or MAI:$PbCl_2$ [21], and $MAPbI_3$ solution [65] for one step spray coating. For example, spray-coating deposition of large band gap $CsPbIBr_2$ thin films has potential for tandem structure devices. This $CsPbIBr_2$ is thermally stable up to 300 °C. For a single-junction device, efficiency reached 6.3% [63]. Other mixed cation and halide perovskite materials could further enhance performance and stability of perovskite solar cell devices [66]. For instance, $FA_{1-x}Cs_xPbI_3$ mixed cation films were prepared with a spray-assisted solution process [64]. Solar cell devices based on this mixed cation film showed enhanced stability and performance compared with those based on $FAPbI_3$. Efficiency increased from 11.3% (for $FAPbI_3$) to 14.2% (for $FA_{0.9}Cs_{0.1}PbI_3$). After aging for 100 h under a relative humidity (RH) of 50%, performance of $FA_{0.9}Cs_{0.1}PbI_3$-based devices remained constant at about 12.5%.

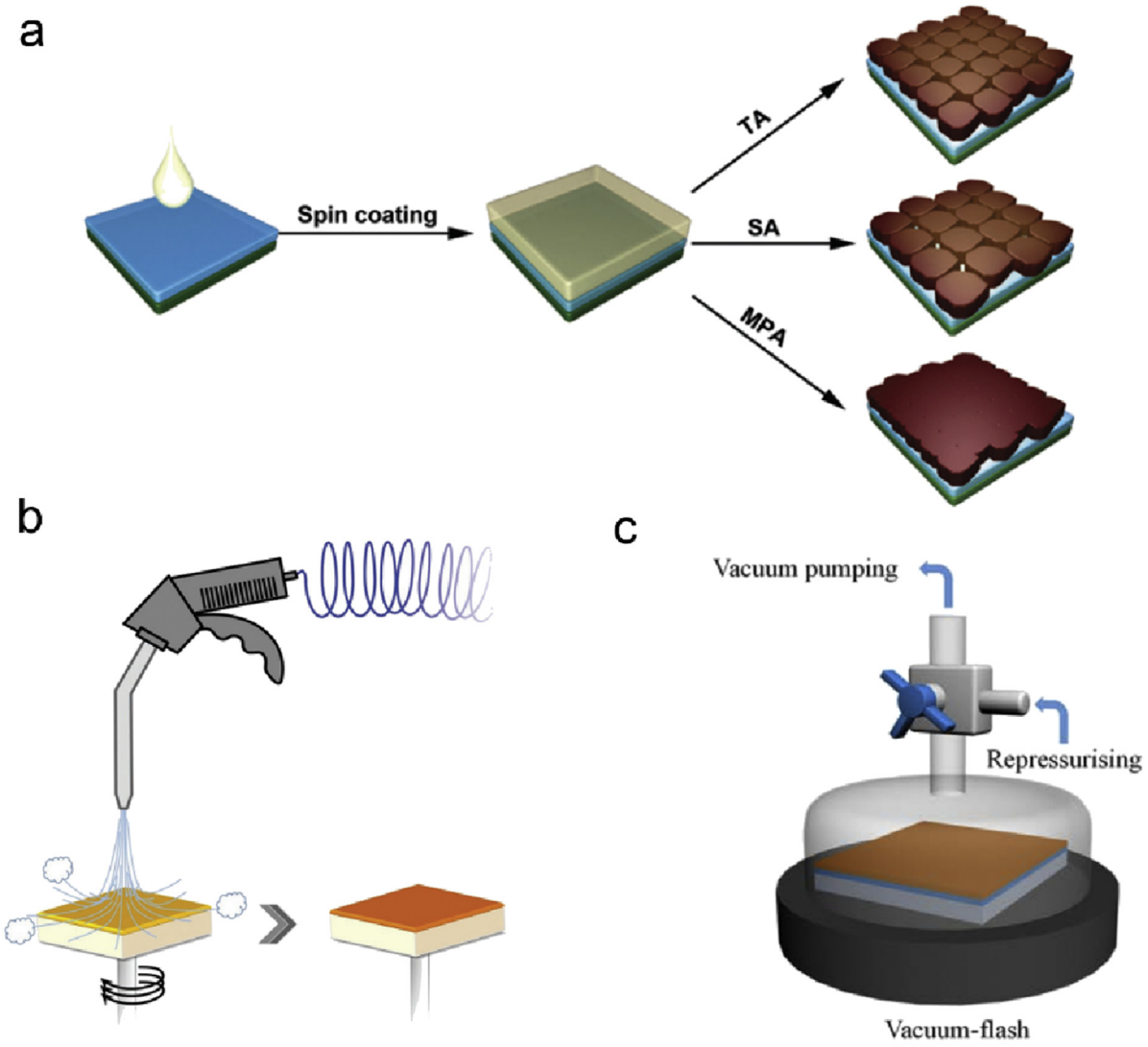

Fig. 3. Post treatments for high-quality perovskite film formation. **a.** Thermal annealing, solvent annealing and MA annealing. Reproduced with permission [46]. Copyright 2016, The Royal Society of Chemistry. **b.** Dry N_2 gas blowing. Reproduced with permission [47]. Copyright 2016, John Wiley and Sons. **c.** Vacuum flash. Reproduced with permission [48]. Copyright 2016, The American Association for the Advancement of Science.

Spray-coating allows fabrication of large area and modules of perovskite solar cells. A two-step, ultrasonic spray coating process was demonstrated for fabrication of large-area, high-efficiency perovskite solar cells with an active area of 1 cm^2 [67]. After optimization of the first step for PbI_2 deposition, choosing a suitable solvent and optimizing concentration and temperature, the PCE of the resulting perovskite solar cells reached 16.03% for a small-area device and 13.09% for a 1-cm^2 device [50]. A more thorough study of an ultrasonic spray coating process, based on *in situ* measurements and modeling of wet film thickness and evaporation rate, offered insight into PbI_2 deposition for high-performance, large-scale perovskite solar cells [67]. For a one-step spray deposition process, pure $MAPbI_{3-x}Cl_x$ powder was first synthesized and dissolved in a mixed solvent of DMF and GBL. By engineering solvent composition and spraying time for deposition, a crystal growth process was developed for depositing perovskite thin films with large grains [68], which are expected to have a lower trap density [69]. As a demonstration, a large-area (100 cm^2) perovskite film was deposited by spray coating. With a geometrical fill factor of 40% (active area = 40 cm^2), module efficiency reached 15.5% [68].

2.3. Doctor blading

Film deposition by doctor blading is simple and low-cost, and can be integrated into roll-to-roll processes for optoelectronic device fabrication (Fig. 2c). Compared with spin coating, there is almost no solution waste when doctor blading is employed. In addition, doctor blading can be operated under ambient conditions. The solution readily wets the substrate with blade movement. Slower solvent evaporation time leads to slower nucleation and crystal growth, resulting in perovskite films with higher coverage and better quality compared to those prepared by spin coating [70]. In this work, the PCE of a device fabricated by spin coating was 1.23% while that prepared with blade coating reached 9.29%. The higher-coverage and higher-quality perovskite film enhances stability of the as-prepared active film and devices. Combining doctor blading with solvent engineering to wash out aqueous-soluble solvent and to form an intermediate phase could further enhance efficiency to 12.21%.

Doctor blading is not only suitable for the perovskite layer, but also for other as well. A device in which doctor blading was used for

sequential deposition of PEDOT:PSS, perovskite, and PCBM under controlled humidity, showed an average efficiency of 10.44% [71]. After modification of the bottom PEDOT:PSS layer by adding poly (4-styrenesulfonic acid), solar cell performance was enhanced by almost 70% (from 6% to 10.15%) [72]. When deposited on cross-linked N4,N4′-bis(4-(6-((3-ethyloxetan-3-yl)methoxy)hexyl)phenyl)−N4,N4′-diphenylbiphenyl-4,4′-diamine-covered ITO substrates, efficiency (15.1%) is higher than PEDOT:PSS-coated substrates (12.8%), illustrating the importance of substrate properties [51]. What is more interesting is that the perovskite film prepared by blade coating showed a carrier diffusion length up to 3.5 μm, which is longer than those of spin-coated films, indicating that blade coating is suitable for formation of large crystalline grains and large-area perovskite cells.

With systematic investigation of how substrate temperature, solution volume, and blade speed relate to film thickness, uniformity, and crystallinity, 1-cm^2 large-area devices with an average efficiency of 7.32% and negligible hysteresis have been fabricated using doctor blading in air [73]. A two-step process is an alternative process to doctor blading. The first step, deposition of PbI_2 with doctor blading, is more controllable. Assisted with air flow, a highly compact layer of PbI_2 was easily obtained. Large solar modules were fabricated and showed efficiencies of 10.4% for solar cell devices with active areas of 10.1 cm^2. Efficiencies of 4.3% were achieved for solar modules with a total area of 100 cm^2 (maximum power 429.7 mW). With a newly developed perovskite precursor ink, large-area, high-quality perovskite films were deposited by doctor blading. For single-junction cells with areas of 1.2 cm^2, efficiency was 15.3% and solar modules with areas of 11.09 cm^2 can achieve efficiencies of 13.3% [58].

2.4. Slot-die coating

Slot-die coating has been widely used for fabricating organic solar cells, and has also been recently introduced into perovskite solar cell fabrication (Fig. 2d) [74,75]. Due to poor film formation by the perovskite precursor solution, a two-step process was employed. First, PbI_2 was applied using slot die coating. Then the PbI_2 was reacted with an MAI solution and was converted to $MAPbI_3$. The state of PbI_2 is critical for the quality of $MAPbI_3$. When PbI_2 films are cloudy, the as-fabricated solar cells show higher PCE (11.96%). Although slot die coating can be integrated into roll-to-roll processing for large-scale flexible modules, the performances of currently reported cells with large areas is relatively low [19]. With the development of charge transport materials, a new hole transport material, π-conjugated 2,2′,7,7′-tetrakis(*N*,*N*-di-*p*-methoxyphenyl)amine-9,9′-bifluorenylidene, with high film-formation capacity compared to that of spiro-MeOTAD, was introduced. A fully slot-die-coated device had an efficiency >14% [76].

2.5. Screen printing

Screen printing is a technique used to coat photo-anodes in dye-sensitized solar cells. Perovskite solar cells could be easily fabricated with a printing process [77,78]. The layer-by-layer printing process starts with screen printing of TiO_2, followed by printing of ZrO_2 and carbon electrodes. Then perovskite solution is dropped onto the porous carbon electrode so that it infiltrates into the mesoporous TiO_2 and ZrO_2. Here ZrO_2 functions as a porous insulating layer to prevent direct contact between the carbon electrode and the TiO_2/FTO substrate. Although it is easy to fabricate solar cells with this printing technique, infiltration of perovskite precursor solution remains a challenge, and is the main reason for lower efficiency compared to those of devices fabricated by other means.

The most intriguing properties of this carbon-coated, printed, mesoscopic device is the high stability and outstanding outdoor performance. A certified PCE of 12.8% and stable performance over >1000 h in ambient air under full sunlight has been recorded for a device with an active area of 0.28 cm^2 [78,79]. This printing process could easily be scaled up. Perovskite solar cell modules with active areas of 31 cm^2 and 70 cm^2 have been fabricated with a large-scale screen printing processes [20]. Efficiencies for 31 cm^2 and 70 cm^2 modules were 10.46% and 10.74%, respectively. Performance was stable at >95% without encapsulation under ambient conditions. Thus, such devices are promising for stable, large-scale solar cell fabrication.

Other than the abovementioned solution processes, ink-jet printing was also investigated; however, so far, it has only been used to make small-area devices [80,81]. Compared with solution processes, dry deposition processes may be more environmental friendly, as they do not require toxic solvents (DMSO, GBL, DMF, chloroform, chlorobenzene, isopropanol, toluene, diethyl ether, etc.), and they are compatible with high-quality, large-area perovskite film deposition, such as vacuum deposition and chemical vapor deposition.

2.6. Vacuum deposition/chemical vapor deposition

Perovskite solar cells are attractive due to their low cost, and they exhibit a large degree of tolerance in synthesis, compared with traditional silicon solar cells or other thin-film solar cells. Perovskite solar cells can also be fabricated using dry processes, such as vacuum deposition or chemical vapor deposition. Furthermore, vacuum deposition is able to fabricate large-area perovskite films with high uniformity (Fig. 4). For example, using hybrid chemical vapor deposition, modules ranging from 1 to 12 cm^2 have been demonstrated [25]. The performance is lower, but reasonable compared with small-area devices. Additionally, the as-fabricated film exhibited higher thermal stability than solution-processed films. Developments and summaries of vacuum deposition/chemical vapor deposition can be found in a recent review [24].

Currently, two reports show particular promise for large-scale perovskite solar cells. Razza et al. demonstrated the largest perovskite film and device to date in literature (100 cm^2) [15]. A second report has a certified module efficiency of 12.1% with an area of 36.13 cm^2 [2]. These devices will be used for the cost-performance analysis in Section 4. With further understanding of perovskite film properties and formation processes, the performance of large-scale perovskite solar cells fabricated using scalable processes is expected to increase to industrial thresholds. Further increases of efficiency and optimization of deposition processes should also help enhance the cost-performance of perovskite solar cells.

Among all the efforts for devices fabrication, the most widely used low cost process for the deposition of high quality perovskite films is still spin-coating process. During the spin coating the excess organic solvents would be removed by a centrifugal force that accelerates the crystallization process. With additive engineering or the anti-solvent process the crystallization process could be further enhanced. However, it is difficult to use spin coating to obtain uniform films over large areas and it is therefore unsuitable for large scale production. Other solution processes including doctor blading, spray coating, slot-die coating and screen printing are proposed to fabricate uniform and large area perovskite films. The slow crystallization process and employment of high boiling point organic solvents cause the formation of microscopic defects and pin-holes that decrease the film quality. As a result, additive engineering was developed to help improve the film quality for this solution process. But the use of toxic solvents in these solution based fabrication processes is still a major obstacle for

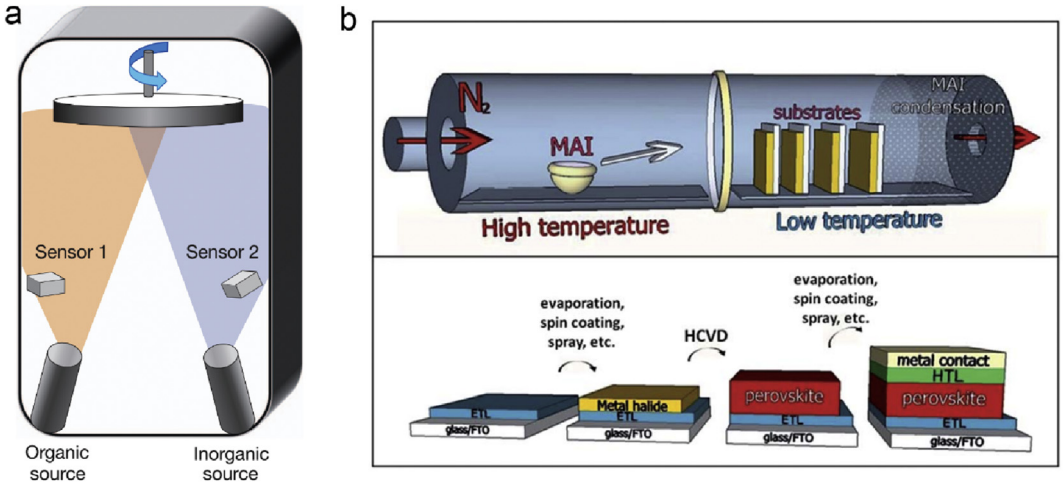

Fig. 4. Dry process for perovskite film deposition. **a.** Dual-source vacuum deposition. Reproduced with permission [82]. Copyright 2014, Nature Publishing Group. **b.** Hybrid chemical vapor deposition process. Reproduced with permission [83]. Copyright 2014, The Royal Society of Chemistry.

commercialization. It has been demonstrated that vacuum deposition can be used to deposit high quality film and eliminate the needs for organic solvents [84,85], although the requirement of high vacuum is expected to increase fabrication cost. Based on these considerations, the CVD process stands out as a highly promising method, which is widely applied in industry, low cost and free of toxic organic solvents. Although at the current stage, the device performance using CVD is still somewhat lower than what has been obtained by other methods, it is expected that with more efforts dedicated to the optimization of the CVD process, better device performance is achievable.

2.7. Large scale deposition of electron transport layer and hole transport layer

Other than the large-scale deposition of perovskite layers, the scalable deposition of charge transport layers is equally important. Unlike the perovskite layer, there are more selections for charge transport layers and therefore it is easier to be compatible with large scale fabrication. The most widely used electron transport layer is TiO_2 which could be deposited by spray coating [86], sputtering coating [87] and screen printing [77], which can be easily scaled up and just retains uniform deposition. The most commonly used hole transport layer is spiro-MeOTAD, which can be deposited via vacuum deposition [88]. The full vacuum deposition process for perovskite solar cells has been demonstrated employing small organic molecule as electron and hole transport layers, which are promising for up-scaling [85,89]. With the development of materials science, more alternatives to conventional electron and hole transport layers are expected to be developed for future commercialization.

3. Lifetime

Although both PCEs and areas of solar cell modules are steadily increasing, the stability and lifetime of perovskite solar cells are still inadequate for practical applications. Achieving long-term stability of perovskite solar cells remains daunting. In addition to considerable research aimed at maximizing efficiency, recent work has also focused on solar cell stability. Several studies have addressed the degradation of perovskite layers and devices [108–110].

Stability problems of perovskite solar cells mainly result from the ambient environment, and from layers adjacent to the perovskite. The perovskite layer is sensitive to oxygen, humidity, heat, and illumination [108,109]. Recently, it was reported that I_2 was generated as a product of $MAPbI_3$ perovskite degradation under a number of conditions, and the generated I_2 further accelerated decomposition of $MAPbI_3$ [111]. The widely employed ZnO reacts with perovskite, causing instability [112,113]. It has been reported that the basic nature of ZnO is the cause for the degradation of $MAPbI_3$ [112]. The thermal decomposition of the perovskite film is driven by acid-base chemistry at the ZnO/$MAPbI_3$ interface. Deprotonation of the MA^+ by the ZnO surface leads to the formation of MA and PbI_2. The basic hydroxyl groups from the ZnO surface further accelerate the decomposition process. More acidic metal oxides such as TiO_2 or SnO_2 can produce perovskite films with better thermal stability [113]. Even the more widely used TiO_2 might also degrade the perovskite layer under UV illumination [114] as can defects [115]. The typically used hole-transport layer, spiro-MeOTAD, and additives also limit long-term stability [116–118]. One of the issues associated with spiro-MeOTAD hole transport layer is its morphology, which can cause perovskite solar cells to degrade. The macro- and micro- pin-holes in spiro-MeOTAD film form channels that facilitate the inward and outward diffusion of gas species [116,117]. A pin-hole free spiro-MeOTAD film can significantly enhance the stability [88,118]. The most widely used ionic dopant lithium bis(trifluoromethanesulfonyl)imide is hygroscopic and the absorption of moisture is the main cause for the instability. Also, it has been reported that the 4-*tert*-Butylpyridine commonly added to spiro-MeOTAD to improve its compositional uniformity [119,120] can dissolve PbI_2 and decompose the perovskite layer [121]. Alternative dopants can enhance the stability. More information about spiro-MeOTAD and its additives can be found from a recently published review article [122]. The most commonly used Au electrode may cause degradation when Au atoms diffuse into the spiro-MeOTAD and perovskite layers under high temperature, which deteriorates performance [123]. Low-cost Ag electrodes readily react with perovskite [124], degrading its performance even in an encapsulated device [125].

At the beginning, perovskite solar cells based on liquid electrolytes exhibited lifetimes of only tens of minutes [7]. With the development of advanced materials and device structures, solar cell stability improved significantly and is gradually approaching commercial levels. With development of mixed-cation and mixed-anion perovskite layers, stability of solar cells is improving, as has been discussed in several recent reviews [66,126]. It is found that

the formation of 2D or 2D/3D perovskite could significantly enhance solar cell stability. The 2D structures show superior moisture stability over 3D MA-based perovskites [127,128]. A recent work by Wang et al. showed high performance perovskite solar cells based on 2D/3D structure with enhanced stability, which retained 80% of the initial efficiency after 1000 h under one sun illumination [129]. Even more impressive, Grancini et al., showed one-year stable perovskite solar modules with zero loss in performance based on 2D/3D $(HOOC(CH_2)_2NH_3)_2PbI_4/MAPbI_3$ perovskite junction and carbon electrode [130]. Device structure may help improve stability, especially in devices with carbon electrodes and hole transport layer-free devices [131]. However, although carbon-based solar cells are promising for long-term stability in harsh environments, their best performance (16%) is still lower than those of other devices [132].

Newly published papers claim stability enhancements using perovskite solar cells. However, procedures to test long-term stability still have not been standardized, making it difficult to compare results of different research groups. It is important to establish a fast and reliable procedure to evaluate the lifetimes of perovskite solar cells, perovskite materials, interface materials, structures, and encapsulation methods. Here we will first summarize the improvements of stability, then we will focus on procedures for testing stability and predicting the life-spans of perovskite solar cells.

There is no standard procedure for measuring long-term stability and/or for predicting device lifetimes under working conditions (Table 2). In most studies, perovskite solar cell stability was reported as the storage time under dark, inert conditions. Such "stability tests" are useless for commercial application, since real solar cells must operate in harsh environments with high humidity, high temperature, intense illumination, and changeable weather. To be meaningful, stability tests must consider all of these factors simultaneously.

Further knowledge can be gained from prior experience with other photovoltaic technologies, where solar cells are subjected to rigorous test conditions to evaluate device lifetimes. Degradation of solar cells comes from two sources. The first is environmental (e.g., temperature, moisture, oxygen, etc.). The second is intrinsic (material and interface chemistries under working conditions). Degradation due the first factor can be minimized with appropriate encapsulation techniques. Thus, to promote stability enhancement, the first step should be encapsulation [79,133]. A second reason for encapsulation is the toxicity of Pb, which will be discussed in Section 5 [38,81,96,114,134–137]. Although research groups worldwide have made progress toward developing alternative Pb-free perovskite solar cells, these devices usually have lower performance.

Normally, in encapsulation, a glass cover with a desiccant and an inert epoxy are used (Fig. 5) [81,133]. The selection of encapsulation method influences the performance after sealing [96]. Sealing processes developed for perovskite solar cells using Surlyn degrade performance due to the heat and pressure of the process. With UV-curable resins, UV-induced degradation could not be prevented. An optimized sealing process is obtained with glass-glass, light-curable methacrylate glue and a Kapton polymer protective layer. With this sealing method a solar cell could be stable under dark conditions longer than 1350 h [96]. After appropriate encapsulation, accelerated lifetime tests could be applied to perovskite solar

Table 2
Long-term stability test for solar cells longer than 500 h.

Solar cell structure	Time (h)	Testing condition					Remaining performance	Ref.
		Light/dark	Temperature (°C)	Atmosphere (Humidity %)	operation	Sealing		
m-TiO_2/ZrO_2/(5-AVA)$_x$(MA)$_{1-x}PbI_3$/Carbon	1008	Light	RT	Air	J-V scan	no	~100%	[78]
m-TiO_2/$MAPbI_3$/sipro-MeOTAD/Au	500	Dark	RT	Air	J-V scan	no	>100%	[6]
m-TiO_2/$MAPbI_3$/spiro-MeOTAD/Au	500	Light	45	Ar	MPP tracking	yes	>80%	[38]
m-Al_2O_3/$MAPbI_{3-x}Cl_x$/spiro-MeOTAD/Au	1000	Light	40	N_2	J-V scan	yes	~50%	[114]
m-TiO_2/$MAPbI_3$/Carbon	>2000	Dark	RT	Air	J-V scan	no	~100%	[152]
m-TiO_2/$MAPbBr_3$/PTAA/Au	2000	Dark	RT	Air	J-V scan	no	>75%	[153]
m-TiO_2/$MAPbI_3$/PDPPDBTE/Au	1000	Dark	RT	Air (20)	J-V scan	no	~100%	[154]
m-TiO_2/$MA_xFA_{1-x}Pb(I_{1-y}Br_y)_3$/spiro-MeOTAD/Au	768	Dark	RT	N_2	J-V scan	no	~100%	[155]
IZO-PET/m-TiO_2/$MAPbI_3$/spiro-MeOTAD/Au	>500	Dark	RT	Air	J-V scan	yes	~100%	[156]
SnO_2/$(FAPbI_3)_{0.85}$-$(MAPbI_3)_{0.15}$/spiro-MeOTAD/Au	~720	Dark	RT	Dry air	J-V scan	no	~97%	[157]
c-TiO_2/PCBB-2CN-2C8/$MAPbI_3$/spiro-MeOTAD/Au	500	Dark	RT	Air (45–50)	J-V scan	no	~65%	[158]
m-TiO_2/$MA_{0.15}FA_{0.81}PbI_{2.51}Br_{0.45}$/spiro-MeOTAD/Au	936	Dark	RT	Air	J-V scan	no	~100%	[98]
ITO/NiOx/$MAPbI_3$/ZnO/Al	~1440	Dark	25	Air (30–35)	J-V scan	no	~90%	[159]
FTO/NiMgLiO/$MAPbI_3$/PCBM/Ti(Nb)O_x/Ag	1000	Light	RT	Air	J-V scan	yes	>90%	[52]
ITO/PEDOT:PSS/$MAPbI_3$/ZnO/Ag	~1000	Dark	30	Air (65)	J-V scan	yes	>95%	[160]
m-TiO_2/ZrO_2/$MAPbI_3$/Carbon	>3000	Dark	RT	Air (35)	J-V scan	no	~100%	[161]
m-TiO_2/$MAPbI_3$/sipro-MeOTAD/Au	>1300	Dark	RT	Air (30)	J-V scan	yes	~97%	[96]
PTAA/$MAPbI_3$/C60/BCP/Cu	816	Dark	RT	Air	J-V scan	no	98%	[162]
c-TiO_2-Cl/$Cs_{0.05}MA_{0.14}FA_{0.81}PbI_{2.55}Br_{0.45}$/spiro-MeOTAD/Au	500	Light (UV cutoff)	RT	N_2	J-V scan and MPP tracking	no	95%	[90]
ITO/NiO//LiF/PC60BM/SnO_2/ZTO/ITO/LiF/Ag	1000	Light	35	Air (40)	MPP tracking	no	~100%	[145]
	1008	Dark	85	Air (85)	MPP tracking	yes	>90%	
m-TiO_2/RbCsMAFAPb$I_{3-x}Br_x$/PTAA/Au	500	Light	85	N_2	MPP tracking	no	95%	[144]
m-TiO_2/$(FAI)_{0.81}(PbI_2)_{0.85}(MABr)_{0.15}(PbBr_2)_{0.15}$:	600	Light	RT	N_2	MPP tracking	no	>95%	[150]
α-bis-PCBM/spiro-MeOTAD/Au	~1050	Dark	RT	Air (40)	J-V scan	no	~95%	
	~1050	Dark	65	Air (40)	J-V scan	no	~90%	
	~480	Dark	85	Air	J-V scan	no	~85%	
FTO/NiO_x/$MAPbI_{3-x}Cl_x$/PCBM:PEI/Ag	1500	Dark	RT	Air (70)	J-V scan	yes	>90%	[49]
m-TiO_2/$MAPbI_3$/Carbon	1002	UV-light	40	Air (45)	J-V scan	yes	~100%	[141]
$BaSnO_3$/$MAPbI_3$/NiO/Au	1000	Light	RT	Air	MPP tracking	yes	93%	[143]
FTO/SnO_2/C60(*N*-DPBI)/$FA_{0.83}Cs_{0.17}Pb(I_{0.6}Br_{0.4})_3$/spiro-OMeTAD/Au	3420	Light	RT	Air	MPP tracking	yes	80%	[163]
m-TiO_2/ZrO_2/(5-AVA)$_x$(MA)$_{1-x}PbI_3$/Carbon	~2160	Dark	80–85	Air	J-V scan	yes	>90%	[79]
	~1056	Light	45	Ar	MPP tracking	yes	~100%	

Here, Light means continuous light-soaking. Dark means storage without illumination. MPP means maximum power point.

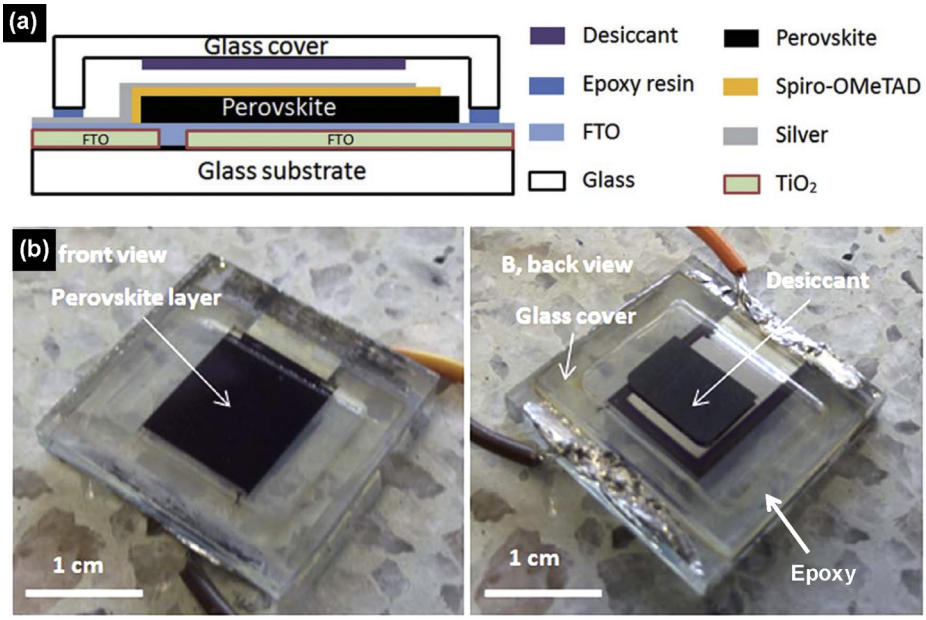

Fig. 5. (a) Side-view schematic of a perovskite solar cell encapsulated with a cover glass, UV-curable epoxy, and desiccant. (b) Photographs of actual devices employing the encapsulation strategy shown in (a). Reprinted with permission [81]. Copyright 2015, The Royal Society of Chemistry.

cells, which would shed light on the intrinsic degradation process of active layers under real world working conditions. However, so far, robust encapsulation materials and methods are still under investigation, but far less attention has been devoted to this subject than to the issue of performance.

For accelerated lifetime measurements, the first consideration is UV light, especially when TiO_2 is employed as the electron transport layer, whether in planar or mesoscopic structures [138,139]. When using a UV filter to get rid of the UV light, a solar cell with a chlorine-passivated TiO_2 compact layer showed much enhanced long-term stability in an inert atmosphere, with <5% loss after continuous maximum power point output tracking [90]. However, UV filters reduce light absorption due to the loss of high-energy photons. One alternative to UV filters is the use of a photocurable fluoropolymer coating outside solar cells [140]. This polymer would first form an efficient hydrophobic barrier against moisture. Secondly, it would absorb UV light and re-emit visible light, so that it would function as a UV filter with almost no loss of light. In continuous UV irradiation aging tests, solar cells with this polymer coating remained stable during 6 months of operation, even under air at 50% RH. In a harsher experiment with carbon-based perovskite solar cell devices, intense, continuous AM1.5-sun equivalent UV light illumination was applied [141]. Solar cells with epoxy protective barriers exhibited remarkable durability with no performance degradation over 1002 h, showing that with some modification, devices can survive under harsh UV light illumination. It has been also found that decayed performance recovered after continuous white light illumination [142]. Because instability under UV light comes from the TiO_2 layer, finding stable, inert alternatives is imperative. Recently, a $BaSnO_3$ electron transport layer has been developed for perovskite solar cells [143]. Unlike TiO_2-based solar cells, devices based on $BaSnO_3$ show much longer lifetimes under full light illumination, including UV light.

The second consideration for long-term stability is high temperature and humidity. Most reports of long-term stability employ room temperature and inert atmospheres. In real-world applications, solar cells can reach 80 °C under illumination. Thus, high-temperature, long-term stability is essential. Normally the maximum working temperature of solar cells is ~45–50 °C. However, higher-temperature, accelerated tests will be helpful to extrapolate the real lifetime of solar cells under working conditions. Recently, with the development of Rb mixed cation perovskite, polymer-coated cells maintained 95% of their initial performance at 85 °C after 500 h under full solar illumination and maximum power point tracking [144]. Due to metal electrode diffusion into perovskite through spiro-MeOTAD under high temperature, PTAA was applied here. Also for real applications, spiro-MeOTAD should be replaced with a more stable material. In another report, with a more stable, inorganic, charge carrier-selective layer, NiO, PCBM, and SnO_2, a stable $Cs_{0.17}FA_{0.83}Pb(Br_{0.17}I_{0.83})_3$ solar cell was fabricated. This device, without encapsulation, withstood a 1000-h damp heat test at 85 °C and 85% RH; however, it was tested in the dark [145].

The third situation to be considered is the repeated light/dark cycle, which causes perovskite solar cell fatigue. According to one report, solar cell performance decreased to <50% of its initial efficiency after dark aging in an open circuit, although performance improves with subsequent continuous illumination [146]. This important behavior has been systematically studied. Lower temperature significantly eliminates the fatigue behavior in dark aging, and it is likely that the cyclic movement of mobile ions causes defects within the perovskite layer, caused by both ionic vacancies and lattice interstitials [146]. In some other reports, perovskite solar cells recovered their initial performance or even improved after dark aging [90,147]. Thus, how this light/dark cycle affects the performance and stability of perovskite solar cells is not yet clear, but this issue is critical, and must be resolved.

However, under all the heat and light conditions employed, there is still no consensus about how to measure and extrapolate the lifetime of perovskite solar cells. The T80 lifetime (defined as the time during which the PCE is ≥80% of the initial value) is widely applied in organic solar cell testing, and is considered the standard for reporting stability performance (Fig. 6) [117,148]. However, with increased solar cell lifetimes, it is difficult to directly track the performance decay as long as 20%. Recently, there was a report about high-temperature (60 °C) lifetime testing and a T80 lifetime

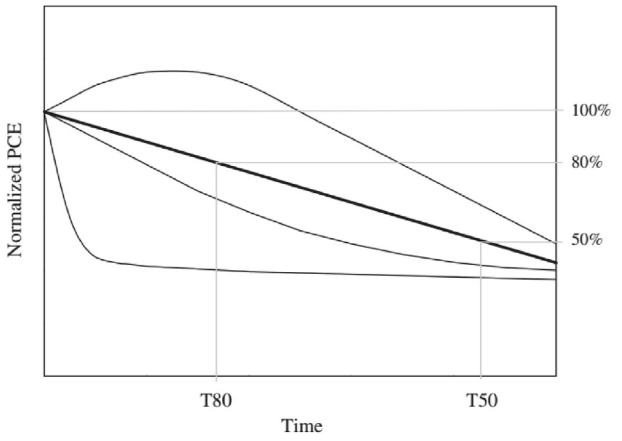

Fig. 6. T80 lifetime definition of solar cells. Reproduced with permission [148]. Copyright 2011, Elsevier.

extrapolated from the linear decay curve. After testing 140 h, the T80 lifetime was estimated to be 580 h [149], but this simple linear extrapolation might not be sufficiently accurate.

To move forward, accelerated tests under harsh conditions should be considered, so as to extrapolate the T80 lifetime under normal operating conditions (light/dark cycling and a 50 °C working temperature). Monitoring solar cell performance decay under accelerated conditions might also provide insights regarding cell degradation mechanisms. For accelerated lifetime testing, it is reasonable to employ procedures like those used to test organic solar cells, with a combination of harsh thermal, humid environments, sunlight illumination and light/dark cycling [148]. The goal is to rigorously test for the same failure mechanisms observed in the field, in a much shorter time. Assuming appropriate encapsulation, most solar cell decay is caused by sunlight and heating.

As an example, we calculate the T80 lifetime of solar cell at 50 °C, based on literature data. A recent report provided performance decay data under different temperatures as accelerated test conditions [150]. However, the test was performed in the dark. Nevertheless, this could be used to extrapolate the storage lifetime (T80) of solar cells at 50 °C (Fig. 7a–c). Here the concept is simply borrowed from organic solar cells [137,151]. Because there is no other stress, but heat, the Arrhenius Model (Eq. (1)) is applied to analyze literature data to predict the storage lifetime (T80) at 50 °C.

$$k_{deg} = A^{*}\exp\left(\frac{-E_a}{k_B T}\right) \quad (1)$$

Here, Ea is the activation energy to be overcome for the degradation process. A first order degradation process is hypothesized and kinetics of the process are temperature-dependent. With a simple calculation, the storage lifetime at 50 °C is extrapolated to be 128 days, or 0.35 year (Fig. 7d). Unfortunately, there are not enough accelerated lifetime measurement data in the literature to accurately predict lifetimes of solar cells under working conditions, at 50 °C, high humidity, under illumination, and in an outdoor environment.

To briefly summarize this section, enhancement of long-term stability of solar cells will undoubtedly depend on the development of advanced materials and device structures. Mixed cation and halide perovskites are being investigated as alternatives to enhance the stability of the perovskite layer. For long-term stability measurements, a universal standard should be adopted in order to understand degradation mechanisms and to compare methods of different research groups. To solve the lifetime issue, an appropriate encapsulation method is required. More stable selective layers and electrodes are also of importance for long life-span perovskite solar cells.

4. Cost-performance analysis

Life-cycle assessment (LCA) has been performed on perovskite solar cells and modules in several reports [9–12,29,30,164,165]. The life cycle of a solar cell was divided into four parts, from raw material, module fabrication, module operation, and disposal, which is the cradle-to-grave lifetime for electronic devices [11,30]. These data are important when considering real world applications and commercialization. As mentioned in the Introduction, to make perovskite solar cells competitive, several goals need to be reached. For example, LCOE for residential usage is expected to be 9.0 cents/kWh by 2020, and that is expected to decline further to 5.0 cents/kWh by 2030 (The SunShot Initiative's 2030 Goal) [1]. To calculate the LCOE for a specific photovoltaic technology, many assumptions have to be made, which can lead to variations from report to report. For example, in a recently report, the LCOE was calculated to be 3.5–4.9 US cents/kWh with an efficiency >12% and lifetime of >15 years [9]. On the other hand, in another report, the analysis showed that even if the cost of the active layers and rear electrode were reduced to zero, a module PCE of 18% and lifetime of 20 years would be required to meet the 9 US cents/kWh target [12]. Nevertheless, the reported calculations provide researchers with some hints about what efficiencies and lifetimes are required for commercialization.

From the energy point of view and not considering the cost of different kinds of energy, Fig. 8a demonstrates an example of the LCA of a 1-m^2 perovskite solar module with an efficiency of 9.1%. An average energy payback time of 0.27 year, equivalent to 1226 h of illumination was calculated [30], which was also demonstrated as feasible when considering long-term stability of perovskite solar cells (Table 2). Furthermore, the energy payback time is much shorter compared with other photovoltaic technologies (Fig. 8c), due to the low-temperature process. As mentioned above, the certified perovskite module exhibited an efficiency of 12.1% with an area of 36.13 cm^2 [2]. Although no standard lifetime was reported, we can assume that the lifetime of solar modules is higher than 1000 h (Table 2). Importantly, even with a lifetime of 1000 h, this module will still generate less energy than is required for fabrication. Therefore, efficiency, scale, and lifetime of perovskite solar cells must still be considerably improved.

Other than solar module efficiency, scale-up, lifetime, cost of materials, fabrication, maintenance, and disposal are equally important. Typically, in all these analyses, the cost could be divided into capital costs, material costs and overhead costs [9,12]. Because fabrication processes for perovskite solar cells share some common features with those of dye-sensitized solar cells, capital costs could be estimated from dye-sensitized solar cells that already have practical value [9]. The capital cost could be further lowered by increasing solar module efficiency and lifetime.

In a normal perovskite solar module, the materials consist of a transparent conductive electrode, electron/hole transport layer, a perovskite layer and a back-contact metal electrode. It is necessary to develop an advanced fabrication process to minimize waste of material [22]. Transparent conductive electrodes are ITO or FTO substrates, and are the most expensive element of perovskite solar modules [29]. In addition, scale-up employing these substrates will significantly lower the module efficiency, due to increased resistance [28]. However, only rarely are alternatives to these transparent electrodes applied and reported [166]. Metal nanowire electrodes hold promise and deserve more attention [167,168]. Another alternative is the use of recycled transparent conductive

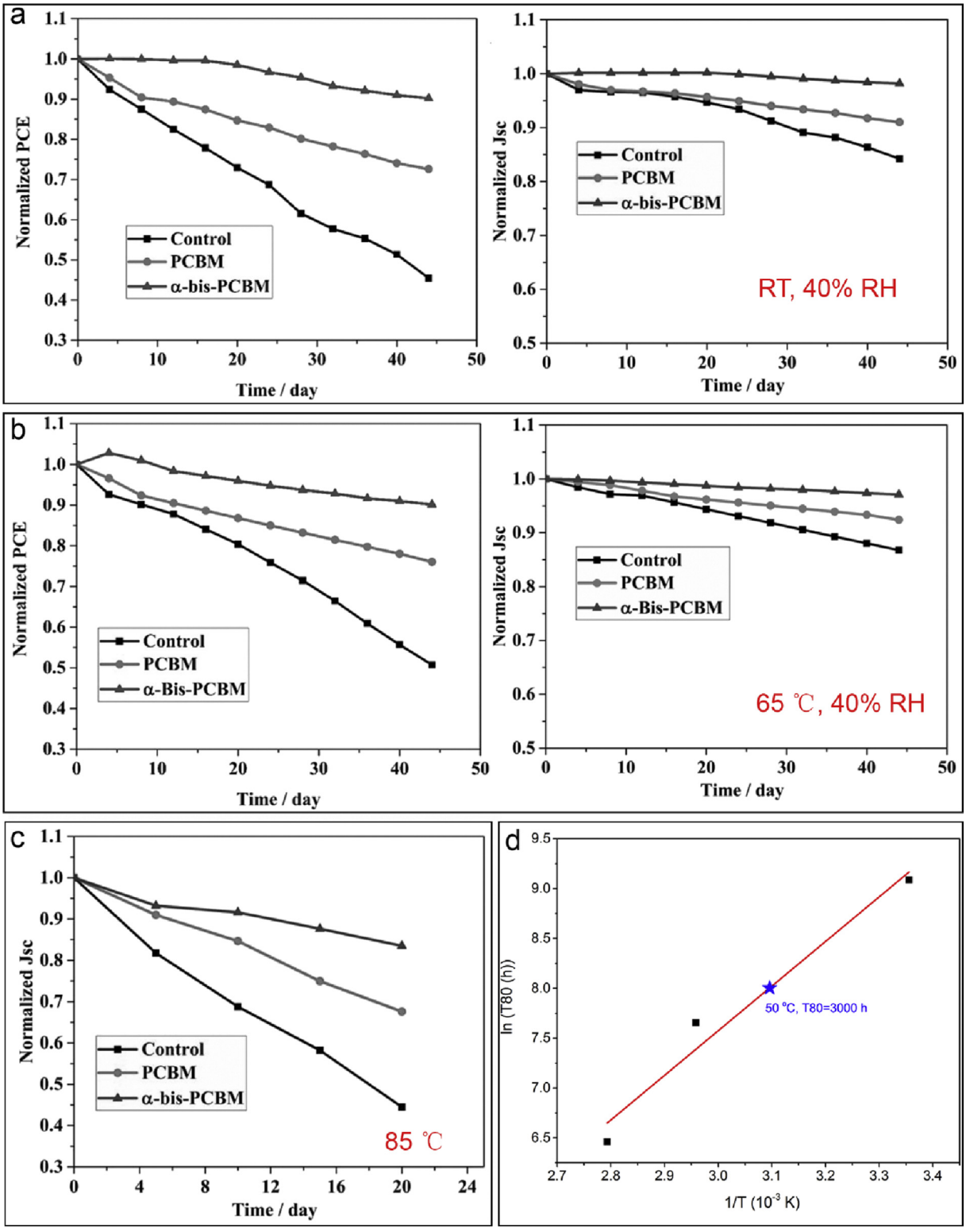

Fig. 7. Accelerated lifetime test of solar cells under different temperatures in a dark environment. a. Data at room temperature. b. Data at 65 °C. c. Data at 85 °C. Reproduced with permission [150]. Copyright 2017, John Wiley and Sons. d. T80 lifetime extrapolated from Arrhenius Model.

electrodes. Perovskite solar cells could be dismantled to recycle the FTO substrate and lead perovskite, which could further lower manufacturing energy consumption, CO_2 emissions, and reducing environmental concerns, but recycling can only be done once there is an active, well-established market for perovskite solar cells (Fig. 8d) [29,165].

The second issue to be addressed is the precious back-contact metal electrode, which is usually gold or silver. Gold is expensive [29] while silver causes degradation of perovskite [81,124]. Recently copper was reported as a suitable back-contact electrode for high-performance, stable perovskite solar cells [162]. The PCE is higher than 20% and remains above 98% after storage under ambient

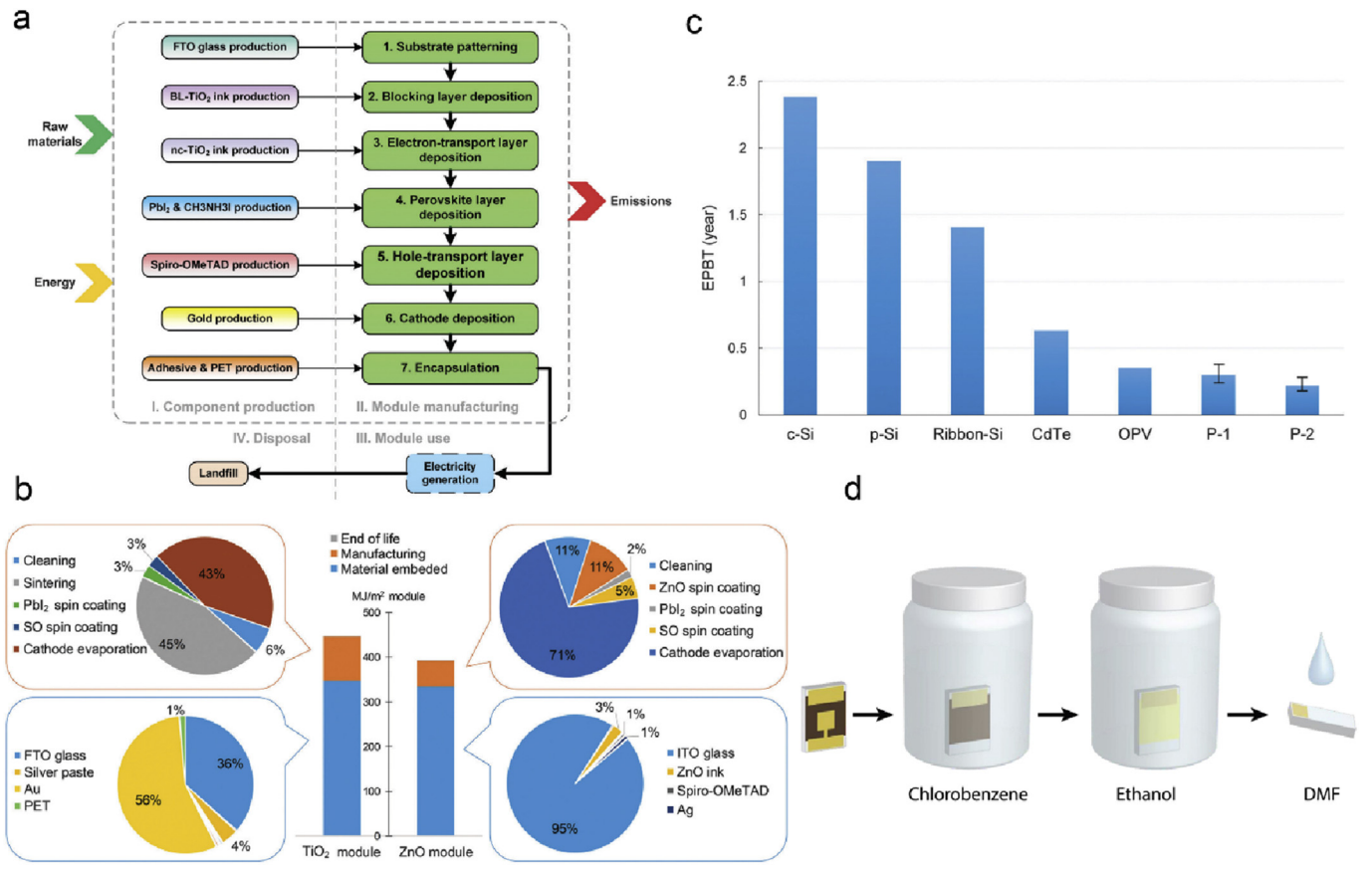

Fig. 8. Life-cycle assessment of perovskite solar cells. **a.** Cradle-to-grave lifetime of perovskite solar modules. **b.** Energy cost assumption of module fabrication process. **c.** Energy payback time (EPBT) of various photovoltaic techniques. Reproduced with permission [30]. Copyright 2015, The Royal Society of Chemistry. **d.** Schematic demonstration of perovskite solar cell recycling. Reproduced with permission [165]. Copyright 2016, The Royal Society of Chemistry.

conditions for 816 h, which is impressive. Another promising alternative is carbon electrodes, which are suitable for low temperatures and for scalable printing processes (Section 2.5). Carbon electrodes are also promising for higher-stability devices (Section 3). However, the efficiency of carbon electrode-based devices must be improved just to catch up with that of current devices.

The main issue that will concern customers, fabricators, and investors is the toxicity and safety of lead-based photovoltaic devices. Toxicity of lead will be discussed in Section 5. To minimize waste and negative effects of lead, recycling of Pb-based perovskite solar cells has been demonstrated and most lead could be recycled [29,165]. However, this is not enough, since leakage of lead during fabrication and maintenance would still exist. The possibility of lead leakage from broken perovskite solar modules will frighten people from purchasing it. There are LCA reports claiming that the lead concentration in perovskite solar module is 0.55%, which is >five times higher than the limits stipulated by the Restriction of Hazardous Substances Directive (RoHS) (0.1%) [10,11]. Deployment will require robust encapsulation materials and methods for both stability and safety.

5. Lead toxicity

The structural and electronic properties of lead-halide-based perovskites for solar energy harvesting applications are remarkable. The photovoltaic community is well aware of the toxicity issues associated with Pb and the anxiety that poses for the public, factors that argue against acceptance of this technology [134,169,170]. Even exposure to very low levels of lead, whether inhaled or ingested, has been associated with significant health problems affecting almost every organ and system in the body (lead poisoning or plumbism) [169–174]. Lead salts (Pb^{2+}) are very quickly and efficiently absorbed by the body. Part of lead's toxicity results from its ability to mimic other metals (e.g. Ca, Fe, Zn) that participate in biological processes. Young children are most vulnerable because the rate of lead uptake is higher due to developmental. The poisonous properties of lead and lead compounds have been documented since ancient times in Greece and Rome [175,176]. In ancient Rome, lead acetate was used to sweeten old wines. Lead-sweetened wine was an important daily consumable for upper-class Romans. Lead was widely used in various applications, including pipes for transporting water and cooking utensils [177]. The synchronous decrease in fertility and the prominence of mental disorders among the Roman aristocracy has been linked to lead poisoning and even speculated as one of the main factors leading to the fall of Rome [175,176]. In modern human history, the complete elimination of lead from gasoline and paints was one of the greatest milestones in public health [178,179]. Specialists reported that billions of people in the world were intoxicated by lead after 1921, when tetraethyl lead was introduced as an antiknock agent in gasoline. Only in 2015, was leaded gasoline scheduled to be phased out in Algeria, the last country still using leaded gasoline [179]. Today, lead remains a persistent toxicant because of omnipresent lead-acid batteries that power more than a billion cars worldwide [179,180]. As reported in recent LCA studies [164,181], lead is one of the most highly recycled materials. The high end-of-life collection and recycling rate make lead batteries one of the few products that can claim a true closed loop. This high recycling rate

has a beneficial impact on the results of LCA, significantly lowering their overall environmental impact [164,181]. Although developed countries have largely eliminated sources of lead contamination, lead poisoning remains a serious concern in developing countries. Dismantling of lead-acid batteries in recycling industries concentrated in many developing countries causes poisoning of whole families, especially children [179,182,183].

5.1. Three-dimensional (3D) halide perovskite

Great efforts have been made to replace Pb with less toxic elements or at least to reduce the level of Pb in the ABX_3 perovskite structure [184,185]. Divalent and heterovalent ions such as Co^{2+}, Fe^{2+}, Ni^{2+}, Zn^{2+} [184,185], Cu^{2+}, Mg^{2+} [185], Sb^{3+} [186], $Sn^{2+,4+}$ [184,185,187], Sr^{2+} [185,187], Cd^{2+} [184,187], Ca^{2+} [187], Mn^{2+} [185,188], Al^{3+} [189], Bi^{3+} [184,190,191], Au^{3+}, In^{3+} [184,191,192], and Ti^{4+} [184] elements have been tried as replacements in perovskites. Although some enhancements in solar cell performance were reported, a general trend of decreased photovoltaic performance with increased bulk doping concentrations of organic-lead-halide perovskites are attributed to increases in carrier recombination and/or phase-segregation phenomena [189,193–196].

Computational approaches based on Goldschmidt's tolerance factor (GTF) are generally employed to predict the geometrical stability of three-dimensional (3D) ABX_3 perovskite structures [197,198]. Based on GTF values calculated for 2352 hypothetical amine-metal-anion permutations, 742 compounds showed GTF values between 0.8 and 1 [199]. It was proposed that >600 unexplored hypothetical compounds could still exist (Fig. 9) [199]. Travis et al. [200] showed that the GTF concept fails to accurately predict the stability of 32 known inorganic iodide perovskites. The chemical properties of heavy iodide anions were shown to be very different from the hard-atomic spheres assumed in the GTF calculations. Using revised ionic radii, which consider greater covalency in metal-halide bonds, they found that only a handful of cations may be successfully placed in the B site of iodide-based perovskite: Sn, Yb, Dy, Tm, Sm, Ca, and Sr. The high moisture sensitivity of Yb, Dy, and Tm, and the wide bandgap formation of Ca and Sr-based iodide perovskites were identified as the main issues for further deployment in photovoltaic applications [200].

Filip and Giustino [201] and Körbel et al. [202] performed a systematic combinatorial search based on density functional calculations (DFT) over the entire periodic table. Starting with over 32,000 possible 3D ABX_3 compounds (Fig. 10a), Körbel et al. found 199 thermodynamically stable perovskites with a cubic structure [202]. Considering the band gap values suitable for photovoltaic applications among these 199 perovskites, except for $BaZrSe_3$, all other ABX_3 structures were based on Sn and Ge halide perovskites. The overall conclusion from these studies is that Pb has the best optoelectronic properties in 3D ABX_3 perovskites. To replace toxic Pb^{2+} while maintaining the high performance is a grand challenge. To decrease the concentration of Pb in the device, a promising way is to mix Sn^{2+} with Pb^{2+} in 3D iodide based perovskite that maintains relatively high performances [203]. However, toxicity of Sn^{2+} has also been reported [169,170]. Chemical composition engineering or alloying [204–206], which employs cation and halide mixing, was recently demonstrated as an effective strategy to tune the optoelectronic and stability properties of Pb-based perovskites [144,163]. However, this strategy has been scarcely explored for Pb-free perovskite systems and further exploration may lead to the discovery of new 3D Pb-free perovskite materials with mixed cations and halides [206].

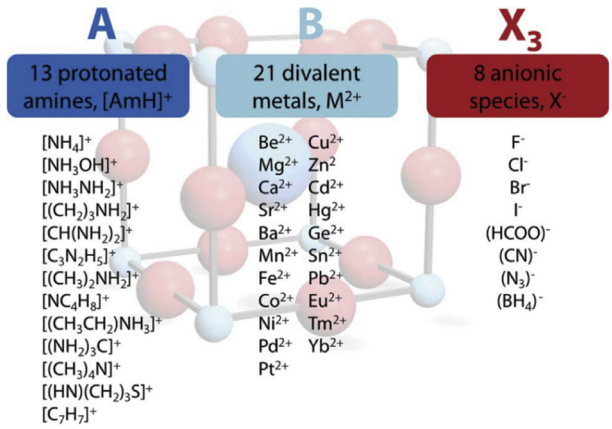

Fig. 9. Goldschmidt's tolerance factors (GTF) for 2352 amine-metal-anion permutations compounds were calculated. Of these, 562 organic anion-based and 180 halide-based compounds lie in the range 0.8 < GTF < 1. Reproduced with permission [199]. Copyright 2015, The Royal Society of Chemistry.

5.2. Two-dimensional (2D), 1D, 0D lead-free halide perovskites

Considering that simple substitution of Pb^{2+} in the ABX_3 structure with alternative divalent cations is challenging (Fig. 10a), another possible approach is to search for multivalent elements yielding a "3-2-9" bilayer (2D) [209–212] (Fig. 10b), bioctahedra (0D), "3-1-5" single-chain, "4-1-6" single-octahedron structures, and "2-1-1-6" 3D double perovskite structures with compensated charges (Fig. 10c) [207,208,213–217]. The size, shape, and functionality of organic cations alter the 3D inorganic network to form extended 2D layers, 1D chains, 0D isolated octahedra or other intermediate cases [218]. In a recent work, Xiao et al. [208] compiled the reported Pb-free halide perovskites and non-perovskites with a wide range of bandgaps and correlated those with structural dimensionality (Fig. 10d). The term non-perovskites corresponds to structures consisting of non-corner-sharing or isolated $[BX_6]$ octahedra. The dimensionality of multilayered perovskites was expressed as 3−1/n (with values between 2 and 3 in the horizontal axis, Fig. 10d). Though most of the reported bandgap values (Fig. 10d) correlate well with structural dimensionality, the same authors introduced the concept of electronic dimensionality, which is associated with the charge transport of photogenerated carriers. Higher electronic dimensionality, accounting for better photovoltaic device performances (Fig. 10e), is associated with isotropic (3D) transport properties, with fewer recombination events in well-ordered structures within the absorber [208]. This may explain the generally lower power conversion efficiencies reported for lower-dimensional perovskites as absorbers: $Cs_3Bi_2I_9$ (2.2 eV Eg, 1.09% PCE) [209], $MA_3Bi_2I_9$ (2.1 eV Eg, 0.26% PCE) [219], $Rb_3Sb_2I_9$ (2.24 eV Eg, 0.66% PCE) [220]. The potential of the split-anion approach is being investigated in the search for Pb-free perovskites [221]. The strategy is to replace Pb with non-toxic Bi in $CH_3NH_3PbI_3$, a high performing perovskite solar cell, by splitting the three I into two I and one Se or S. $CH_3NH_3BiSI_2$ was shown to be a promising perovskite absorber material [221]. A similar strategy was used by Cortecchia et al. [222] to synthesize 2D copper perovskites as light harvesters having the general formula of $MA_2CuCl_xBr_{4-x}$. Pb-free perovskites with mixed chalcogen and halogen anions, $AB(Ch,X)_3$ (A = Cs or Ba; B = Sb or Bi; Ch = O, S, Se, Te; and X = F, Cl, Br, I), have also been described by Hong et al. [223].

5.3. Double perovskites

3D double perovskite structures (also called elpasolites) with a general formula unit $A_2B'B''X_6$, which are formed by substitution of a pair of B′ and B″ elements in the B-site (Fig. 10d) have received much attention as promising absorber materials

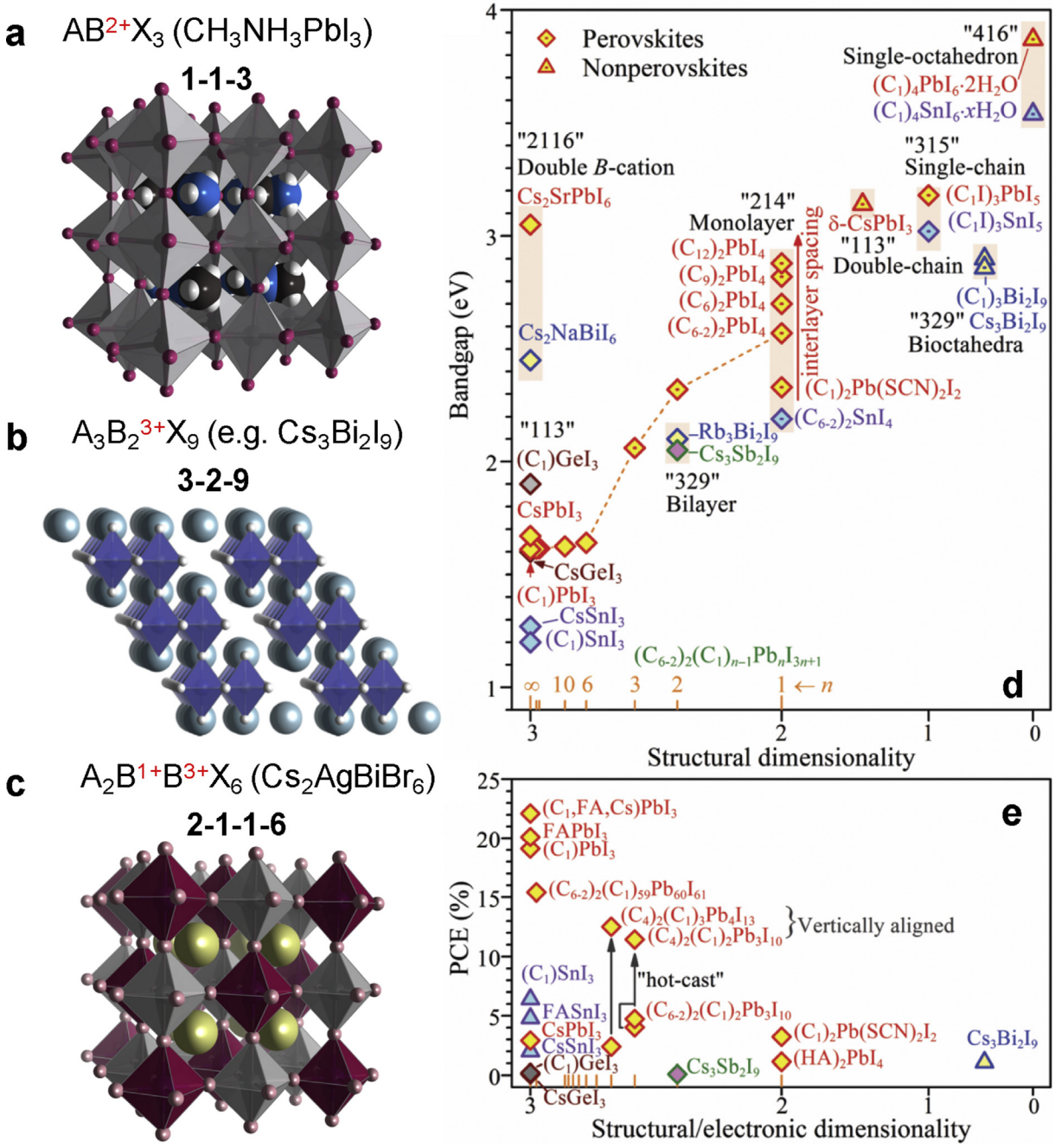

Fig. 10. Polyhedral models of (a) ABX_3 or "1-1-3" structure (e.g. $CH_3NH_3PbI_3$); (b) $A_3B_2X_9$ or "3-2-9" with lower-dimensionality structure (e.g. $Cs_3Bi_2I_9$); and (c) $A_2B'B''X_6$ or "2-1-1-6" chess-type structure (e.g. $Cs_2AgBiBr_6$). Reproduced with permission [207]. Copyright 2016, American Chemical Society. (d) Optical bandgaps of selected iodide-based perovskites as a function of crystal dimensionality. (e) The highest reported power conversion efficiencies for selected iodide-based perovskites. Red, violet, purple, blue, and olive symbols indicate Pb-, Sn-, Ge-, Bi-, Sb-based halides, respectively. "C_n" indicates $C_nH_{2n+1}NH_3$, "$C_{6\text{-}2}$" indicates $C_6H_5(CH_2)_2NH_3$, "C_1I" indicates $NH_2C(I)=NH_2$, "FA" indicates $HC(NH_2)_2$, and "HA" indicates $C_5N_3H_{11}$. Reproduced with permission [208]. Copyright 2017, The Royal Society of Chemistry. (For interpretation of the references to colour in this figure legend, the reader is referred to the web version of this article.)

[207,213–217,224,225]. Metals with oxidation states of 2+/2+ and 1+/3+ in the B′/B″ sites can be accommodated in double perovskites. Although PCEs have not been reported, examples of compounds promising for photovoltaic applications include: $Cs_2Ag^{1+}Bi^{3+}X_6$ (X = Br and Cl) [213,214,225], Cs_2NaBiI_6 [208], Cs_2InBiX_6 (X = Br and Cl) [225], and $(MA)_2KBiCl_6$ [215]. Elements with tetravalent cations can also be incorporated to form 4+/0 double perovskites, where the B′ site would be vacant. $Cs_2Sn^{4+}I_6$ adopts this structure and has been explored as a hole transport layer in dye-sensitized solar cells [211,212,226]. Further work remains to be done in order to explore the potential of lead-free double perovskites for photovoltaic applications. Computational screening procedures are ideally positioned to search for new structurally stable double perovskites. Volonakis et al. [216] proposed a new family of Pb-free inorganic halide double perovskites $A_2B'B''X_6$ based on A = Cs, B′ = Au, Ag, Cu, B″ = Bi or Sb, and X = Cl, Br, I using first-principle calculations that exhibit promising optoelectronic properties. So far, working solar cells based on double

perovskites have not been reported. This has mostly been attributed due to difficulties in developing synthetic routes to obtain uniform thin films of the correct phase and composition [207,208,216,217,225].

6. Summary, future direction, and challenges

There is no doubt that exceptional solar-to-electricity power conversion efficiencies can be achieved based on metal-halide perovskites solar cells [2,227]. Furthermore, the optimal band gap for a single-junction solar cell is between 1.1 eV and 1.4 eV, as dictated by the Shockley–Queisser limit [228]; therefore numerous improvements are expected to achieve even higher efficiencies [228]. However, current state-of-the-art perovskite solar cells have relatively small active areas (~0.1 cm^2). Based on our survey (Table 1), the total number of reports of perovskite solar cells employing active areas >1 cm^2 is still limited (1 cm^2 is not considered "large" by industrial standards). Further efforts to produce large-area perovskite solar cells are much needed. As mentioned previously, (i) low cost, (ii) large area, (iii) high throughput, (iv) high solar-to-energy PCE, (v) reproducibility, (vi) cost performance, (vii) long lifetime, and (viii) low toxicity (or environmental impact) are key parameters for advancing a photovoltaic technology from laboratory-scale fabrication to industrial-scale applications [1,12–14,27,229–234]. With regard to points (i) to (vi) above, various perovskite thin-film deposition technologies such as spin-coating, doctor blading, slot-die coating, printing, spray-deposition, soft-cover deposition, dip coating, and vapor-based deposition have been developed (Section 2 and Table 1). The first step, fabrication of large-area perovskite films with high quality (i.e. high film uniformity, reduced roughness across the whole area, reduced density of structural defects such as pinholes, etc.), is essential for industrial applications. The second step involves fabrication of modules and the third step consists of integrating modules into a panel. From our perspective, two reports present state-of-the-art perovskite solar cells. The largest perovskite film and device in the literature boasts an area of 100 cm^2 [15]. A second report has a certified module efficiency of 12.1% with an area of 36.13 cm^2 [2]. These reports show promise that large-area perovskite solar cells can be used as components to fabricate panels (Fig. 1). Although the raw materials of which perovskite solar cells are comprised, are relatively inexpensive and abundant, currently reported cost-performance analysis concludes that much work is still needed to make perovskite solar cell technology competitive [9–11]. LCOE and LCA parameters are important standard parameters for comparing different photovoltaic technologies (Sections 1 and 4). This analysis is complex, since thresholds may vary according to governmental policies, subsidies, investors, societal demands for energy, environmental impacts, and so on [1]. For instance, considering the U.S. Department of Energy (DOE) SunShot 2020 goals, the defined LCOE is 9 cents/kWh by 2020, expected to eventually reach 5 cents/kWh by 2030. Cai et al. [9] predicted an LCOE of 3.5–4.9 cents/kWh if perovskite solar cell modules (1 m^2) achieve 12% efficiency and a life span of 15 years. Similarly, Chang et al. [12] calculated that a perovskite module efficiency of 18% and a lifespan of 20 years would be required to attain 9 cents/kWh.

Long-term stability of perovskite solar cells has been daunting. Perovskite stability under thermal stress is particularly important for solar cell operation following IEC 61646/IEC 61215 protocols [235]; for industrially relevant certification, solar modules must be able to operate successfully between −40 °C and +85 °C. Saliba et al. [144] fabricated devices with an architecture of FTO/c-TiO_2/mp-TiO_2/$Rb_{0.05}Cs_{0.05}(FA_{0.83}MA_{0.17})_{0.90}Pb(I_{0.83}Br_{0.17})_3$/PTAA/Au showing the best stabilized efficiencies of up to 21.6% (averaged PCE was 20.2%). Furthermore, PTAA employed as hole transport layer (HTL) helped these cells maintain ~95% of their initial performance when tested in an N_2 atmosphere, but at a temperature of 85 °C for 500 h and under operational conditions (full illumination and tracking the maximum power point). Wang et al. [163] showed that an FTO/SnO_2/C60/$Cs_{0.17}FA_{0.83}Pb(I_{0.6}Br_{0.4})_3$/spiro-MeOTAD/Au device architecture was able to achieve an efficiency of 18.3%, as well as a post burn-in T80 over 3420 h when aged under continuous full-spectrum solar illumination (i.e. without a UV filter) in air. Newly published papers claim stability enhancements of perovskite solar cells (Table 2). However, in our view, a standard protocol to test the long-term stability (quantification/extrapolation methodologies) under working conditions so that comparisons can be made among different groups worldwide is still lacking. In most published data, device lifetimes were reported as the storage time in a dark, inert atmosphere. Current stability tests may provide some clues about device stabilities, but they are useless when considering commercial applications. Real solar cells are operated in harsh environments with high humidity, high temperature, and full solar illumination with varying weather conditions. It is important to establish a fast and reliable protocol for the lifetime analysis of perovskite solar cells, allowing scientists and fabricators to evaluate and predict the quality and stability of newly proposed perovskite materials and devices. In this sense, the *Reporting Checklist for Solar Cell Manuscripts* sheet proposed by Nature Publishing Group may be effective.

The third issue that most concerns investors and costumers is the toxicity of lead, where handling mistakes during fabrication, installation, or disposal phase may cause severe damage to the environment and to human beings. In addition to environmental impacts, evaluation of energy-intensive steps need to be identified when considering perovskite photovoltaic technology entries into the global market. It has been widely accepted that the majority of technology's environmental impact comes during the design and development stage, and it is effective to perform a comprehensive LCA in the early stage of technology development to further guide sustainability of this technology [9–12,29,30,164,165]. In the LCA methodology, a detailed material inventory table, such as the mass of raw materials, energy consumption for fabrication of individual layers, and direct CO_2 emissions from raw material extraction, module fabrication, module operation and disposal (the cradle-to-grave lifetime), are all considered. Based on surveyed reports, to further develop advanced fabrication processes, minimizing material costs and lessening environment impacts, the following actions may need to be considered: (i) avoid the use of ITO or FTO, which apart from its high cost, has high environment impact (CO_2 emissions) and is the cause of lower efficiencies due to increased series resistance; (ii) avoid the use of Au or Ag as a back contact (carbon electrodes are promising alternatives); (iii) HTL-free perovskite solar cells are desirable; (iv) development of recycling strategies [29,165,236] (v) employment of less-toxic solvents [237] (vi) estimated lead concentration in a perovskite module (0.55%) is higher than the stipulated RoHS (0.1%), encouraging development of lead-free absorber materials; (vii) encapsulation will increase over-all cost. Perovskite compounds based on Bi^{3+} with lone-pair electronics similar to those of Pb^{2+} are reported to be potential alternative candidates (Section 5). Current lead-free perovskites exhibit far inferior solar cell performance compared to lead-based counterparts. This invites more concerted research efforts to develop new alternative perovskites that will make this technology more attractive to industry.

Acknowledgements

This work was supported by funding from the Energy Materials and Surface Sciences Unit of the Okinawa Institute of Science and

Technology Graduate University, the OIST R&D Cluster Research Program, the OIST Proof of Concept (POC) Program and JSPS KAKENHI Grant Number 15K17925. We thank Steven D. Aird, Technical Editor at Okinawa Institute of Science and Technology Graduate University for editing the manuscript.

References

[1] S. Chu, Y. Cui, N. Liu, The path towards sustainable energy, Nat. Mater. 16 (2017) 16–22.
[2] M.A. Green, K. Emery, Y. Hishikawa, W. Warta, E.D. Dunlop, D.H. Levi, A.W.Y. Ho-Baillie, Solar cell efficiency tables (version 49), Prog. Photovolt. Res. Appl. 25 (2017) 3–13.
[3] Y. Lin, B. Chen, F. Zhao, X. Zheng, Y. Deng, Y. Shao, Y. Fang, Y. Bai, C. Wang, J. Huang, Matching charge extraction contact for wide-bandgap perovskite solar cells, Adv. Mater. 29 (2017) 1700607.
[4] M.A. Green, K. Emery, Y. Hishikawa, W. Warta, E.D. Dunlop, Solar cell efficiency tables (version 48), Prog. Photovolt. Res. Appl. 24 (2016) 905–913.
[5] W.S. Yang, J.H. Noh, N.J. Jeon, Y.C. Kim, S. Ryu, J. Seo, S.I. Seok, High-performance photovoltaic perovskite layers fabricated through intramolecular exchange, Science 348 (2015) 1234–1237.
[6] H.-S. Kim, C.-R. Lee, J.-H. Im, K.-B. Lee, T. Moehl, A. Marchioro, S.-J. Moon, R. Humphry-Baker, J.-H. Yum, J.E. Moser, M. Grätzel, N.-G. Park, Lead iodide perovskite sensitized all-solid-state submicron thin film mesoscopic solar cell with efficiency exceeding 9%, Sci. Rep. 2 (2012) 591.
[7] A. Kojima, K. Teshima, Y. Shirai, T. Miyasaka, Organometal halide perovskites as visible-light sensitizers for photovoltaic cells, J. Am. Chem. Soc. 131 (2009) 6050–6051.
[8] Perovskite-info, http://www.perovskite-info.com/companies/perovskite-solar-panels-developers (Accessed 1 May 2017).
[9] M. Cai, Y. Wu, H. Chen, X. Yang, Y. Qiang, L. Han, Cost-performance analysis of perovskite solar modules, Adv. Sci. (2016) 1600269.
[10] N. Espinosa, L. Serrano-Lujan, A. Urbina, F.C. Krebs, Solution and vapour deposited lead perovskite solar cells: ecotoxicity from a life cycle assessment perspective, Sol. Energy Mater. Sol. Cells 137 (2015) 303–310.
[11] L. Serrano-Lujan, N. Espinosa, T.T. Larsen-Olsen, J. Abad, A. Urbina, F.C. Krebs, Tin- and lead-based perovskite solar cells under scrutiny: an environmental perspective, Adv. Energy Mater. 5 (2015) 1501119.
[12] N.L. Chang, A.W. Yi Ho-Baillie, P.A. Basore, T.L. Young, R. Evans, R.J. Egan, A manufacturing cost estimation method with uncertainty analysis and its application to perovskite on glass photovoltaic modules, Prog. Photovolt. Res. Appl. 25 (2017) 390–405.
[13] Q. Lin, R.C.R. Nagiri, P.L. Burn, P. Meredith, Considerations for upscaling of organohalide perovskite solar cells, Adv. Opt. Mater. 5 (2017) 1600819.
[14] A.A. Asif, R. Singh, G.F. Alapatt, Technical and economic assessment of perovskite solar cells for large scale manufacturing, J. Renew. Sustain. Energy 7 (2015) 043120.
[15] S. Razza, F. Di Giacomo, F. Matteocci, L. Cinà, A.L. Palma, S. Casaluci, P. Cameron, A. D'Epifanio, S. Licoccia, A. Reale, T.M. Brown, A. Di Carlo, Perovskite solar cells and large area modules (100 cm^2) based on an air flow-assisted PbI_2 blade coating deposition process, J. Power Sources 277 (2015) 286–291.
[16] Y.-C. Chern, H.-R. Wu, Y.-C. Chen, H.-W. Zan, H.-F. Meng, S.-F. Horng, Reliable solution processed planar perovskite hybrid solar cells with large-area uniformity by chloroform soaking and spin rinsing induced surface precipitation, AIP Adv. 5 (2015) 087125.
[17] Y. Wang, J. Luo, R. Nie, X. Deng, Planar perovskite solar cells using $CH_3NH_3PbI_3$ films: a simple process suitable for large-scale production, Energy Technol. 4 (2016) 473–478.
[18] C.-H. Chiang, J.-W. Lin, C.-G. Wu, One-step fabrication of a mixed-halide perovskite film for a high-efficiency inverted solar cell and module, J. Mater. Chem. A 4 (2016) 13525–13533.
[19] K. Hwang, Y.-S. Jung, Y.-J. Heo, F.H. Scholes, S.E. Watkins, J. Subbiah, D.J. Jones, D.-Y. Kim, D. Vak, Toward large scale roll-to-roll production of fully printed perovskite solar cells, Adv. Mater. 27 (2015) 1241–1247.
[20] A. Priyadarshi, L.J. Haur, P. Murray, D. Fu, S. Kulkarni, G. Xing, T.C. Sum, N. Mathews, S.G. Mhaisalkar, A large area (70 cm^2) monolithic perovskite solar module with a high efficiency and stability, Energy Environ. Sci. 9 (2016) 3687–3692.
[21] A.T. Barrows, A.J. Pearson, C.K. Kwak, A.D.F. Dunbar, A.R. Buckley, D.G. Lidzey, Efficient planar heterojunction mixed-halide perovskite solar cells deposited via spray-deposition, Energy Environ. Sci. 7 (2014) 2944–2950.
[22] F. Ye, H. Chen, F. Xie, W. Tang, M. Yin, J. He, E. Bi, Y. Wang, X. Yang, L. Han, Soft-cover deposition of scaling-up uniform perovskite thin films for high cost-performance solar cells, Energy Environ. Sci. 9 (2016) 2295–2301.
[23] T. Liu, K. Chen, Q. Hu, R. Zhu, Q. Gong, INverted perovskite solar cells: progresses and perspectives, Adv. Energy Mater. 6 (2016) 1600457.
[24] L.K. Ono, M.R. Leyden, S. Wang, Y.B. Qi, Organometal halide perovskite thin films and solar cells by vapor deposition, J. Mater. Chem. A 4 (2016) 6693–6713.
[25] M.R. Leyden, Y. Jiang, Y.B. Qi, Chemical vapor deposition grown formamidinium perovskite solar modules with high steady state power and thermal stability, J. Mater. Chem. A 4 (2016) 13125–13132.
[26] Y. Zhou, K. Zhu, Perovskite solar cells shine in the "valley of the sun", ACS Energy Lett. 1 (2016) 64–67.
[27] Y. Galagan, E.W.C. Coenen, W.J.H. Verhees, R. Andriessen, Towards the scaling up of perovskite solar cells and modules, J. Mater. Chem. A 4 (2016) 5700–5705.
[28] M. Hambsch, Q. Lin, A. Armin, P.L. Burn, P. Meredith, Efficient, monolithic large area organohalide perovskite solar cells, J. Mater. Chem. A 4 (2016) 13830–13836.
[29] A. Binek, M.L. Petrus, N. Huber, H. Bristow, Y. Hu, T. Bein, P. Docampo, Recycling perovskite solar cells to avoid lead waste, ACS Appl. Mater. Interfaces 8 (2016) 12881–12886.
[30] J. Gong, S.B. Darling, F. You, Perovskite photovoltaics: life-cycle assessment of energy and environmental impacts, Energy Environ. Sci. 8 (2015) 1953–1968.
[31] J.H. Heo, D.H. Song, S.H. Im, Planar $CH_3NH_3PbBr_3$ hybrid solar cells with 10.4% power conversion efficiency, fabricated by controlled crystallization in the spin-coating process, Adv. Mater. 26 (2014) 8179–8183.
[32] G.E. Eperon, V.M. Burlakov, P. Docampo, A. Goriely, H.J. Snaith, Morphological control for high performance, solution-processed planar heterojunction perovskite solar cells, Adv. Func. Mater. 24 (2014) 151–157.
[33] A. Dualeh, N. Tétreault, T. Moehl, P. Gao, M.K. Nazeeruddin, M. Grätzel, Effect of annealing temperature on film morphology of organic–inorganic hybrid pervoskite solid-state solar cells, Adv. Func. Mater. 24 (2014) 3250–3258.
[34] D.T. Moore, H. Sai, K.W. Tan, D.-M. Smilgies, W. Zhang, H.J. Snaith, U. Wiesner, L.A. Estroff, Crystallization kinetics of organic–inorganic trihalide perovskites and the role of the lead anion in crystal growth, J. Am. Chem. Soc. 137 (2015) 2350–2358.
[35] P.-W. Liang, C.-Y. Liao, C.-C. Chueh, F. Zuo, S.T. Williams, X.-K. Xin, J. Lin, A.K.Y. Jen, Additive enhanced crystallization of solution-processed perovskite for highly efficient planar-heterojunction solar cells, Adv. Mater. 26 (2014) 3748–3754.
[36] W. Zhang, M. Saliba, D.T. Moore, S.K. Pathak, M.T. Hörantner, T. Stergiopoulos, S.D. Stranks, G.E. Eperon, J.A. Alexander-Webber, A. Abate, A. Sadhanala, S. Yao, Y. Chen, R.H. Friend, L.A. Estroff, U. Wiesner, H.J. Snaith, Ultrasmooth organic–inorganic perovskite thin-film formation and crystallization for efficient planar heterojunction solar cells, Nat. Commun. 6 (2015) 6142.
[37] Y. Wu, F. Xie, H. Chen, X. Yang, H. Su, M. Cai, Z. Zhou, T. Noda, L. Han, Thermally stable $MAPbI_3$ perovskite solar cells with efficiency of 19.19% and area over 1 cm^2 achieved by additive engineering, Adv. Mater. 29 (2017) 1701073.
[38] J. Burschka, N. Pellet, S.-J. Moon, R. Humphry-Baker, P. Gao, M.K. Nazeeruddin, M. Gratzel, Sequential deposition as a route to high-performance perovskite-sensitized solar cells, Nature 499 (2013) 316–319.
[39] M. Xiao, F. Huang, W. Huang, Y. Dkhissi, Y. Zhu, J. Etheridge, A. Gray-Weale, U. Bach, Y.-B. Cheng, L. Spiccia, A fast deposition-crystallization procedure for highly efficient lead iodide perovskite thin-film solar cells, Angew. Chem. Int. Ed. 53 (2014) 9898–9903.
[40] N.J. Jeon, J.H. Noh, Y.C. Kim, W.S. Yang, S. Ryu, S.I. Seok, Solvent engineering for high-performance inorganic–organic hybrid perovskite solar cells, Nat. Mater. 13 (2014) 897–903.
[41] N. Ahn, D.-Y. Son, I.-H. Jang, S.M. Kang, M. Choi, N.-G. Park, Highly reproducible perovskite solar cells with average efficiency of 18.3% and best efficiency of 19.7% fabricated via Lewis base adduct of lead(II) iodide, J. Am. Chem. Soc. 137 (2015) 8696–8699.
[42] H. Zhou, Q. Chen, G. Li, S. Luo, T.-b. Song, H.-S. Duan, Z. Hong, J. You, Y. Liu, Y. Yang, Interface engineering of highly efficient perovskite solar cells, Science 345 (2014) 542–546.
[43] Z. Xiao, C. Bi, Y. Shao, Q. Dong, Q. Wang, Y. Yuan, C. Wang, Y. Gao, J. Huang, Efficient, high yield perovskite photovoltaic devices grown by interdiffusion of solution-processed precursor stacking layers, Energy Environ. Sci. 7 (2014) 2619–2623.
[44] C. Bi, Y. Shao, Y. Yuan, Z. Xiao, C. Wang, Y. Gao, J. Huang, Understanding the formation and evolution of interdiffusion grown organolead halide perovskite thin films by thermal annealing, J. Mater. Chem. A 2 (2014) 18508–18514.
[45] Z. Xiao, Q. Dong, C. Bi, Y. Shao, Y. Yuan, J. Huang, Solvent annealing of perovskite-induced crystal growth for photovoltaic-device efficiency enhancement, Adv. Mater. 26 (2014) 6503–6509.
[46] Y. Jiang, E.J. Juarez-Perez, Q. Ge, S. Wang, M.R. Leyden, L.K. Ono, S.R. Raga, J. Hu, Y.B. Qi, Post-annealing of $MAPbI_3$ perovskite films with methylamine for efficient perovskite solar cells, Mater. Horiz. 3 (2016) 548–555.
[47] B. Conings, A. Babayigit, M.T. Klug, S. Bai, N. Gauquelin, N. Sakai, J.T.-W. Wang, J. Verbeeck, H.-G. Boyen, H.J. Snaith, A universal deposition protocol for planar heterojunction solar cells with high efficiency based on hybrid lead halide perovskite families, Adv. Mater. 28 (2016) 10701–10709.
[48] X. Li, D. Bi, C. Yi, J.D. Decoppet, J. Luo, S.M. Zakeeruddin, A. Hagfeldt, M. Gratzel, A vacuum flash-assisted solution process for high-efficiency large-area perovskite solar cells, Science 353 (2016) 58–62.
[49] H.-C. Liao, P. Guo, C.-P. Hsu, M. Lin, B. Wang, L. Zeng, W. Huang, C.M.M. Soe, W.-F. Su, M.J. Bedzyk, M.R. Wasielewski, A. Facchetti, R.P.H. Chang, M.G. Kanatzidis, T.J. Marks, Enhanced efficiency of hot-cast large-area planar perovskite solar cells/modules having controlled chloride incorporation, Adv. Energy Mater. 7 (2017) 1601660.
[50] H. Huang, J. Shi, L. Zhu, D. Li, Y. Luo, Q. Meng, Two-step ultrasonic spray deposition of $CH_3NH_3PbI_3$ for efficient and large-area perovskite solar cell, Nano Energy 27 (2016) 352–358.

[51] Y. Deng, E. Peng, Y. Shao, Z. Xiao, Q. Dong, J. Huang, Scalable fabrication of efficient organolead trihalide perovskite solar cells with doctor-bladed active layers, Energy Environ. Sci. 8 (2015) 1544–1550.

[52] W. Chen, Y. Wu, Y. Yue, J. Liu, W. Zhang, X. Yang, H. Chen, E. Bi, I. Ashraful, M. Grätzel, L. Han, Efficient and stable large-area perovskite solar cells with inorganic charge extraction layers, Science 350 (2015) 944–948.

[53] Y. Wu, X. Yang, W. Chen, Y. Yue, M. Cai, F. Xie, E. Bi, A. Islam, L. Han, Perovskite solar cells with 18.21% efficiency and area over 1 cm^2 fabricated by heterojunction engineering, Nat. Energy 1 (2016) 16148.

[54] J. Seo, S. Park, Y. Chan Kim, N.J. Jeon, J.H. Noh, S.C. Yoon, S.I. Seok, Benefits of very thin PCBM and LiF layers for solution-processed p-i-n perovskite solar cells, Energy Environ. Sci. 7 (2014) 2642–2646.

[55] Y. Yuan, G. Giri, A.L. Ayzner, A.P. Zoombelt, S.C.B. Mannsfeld, J. Chen, D. Nordlund, M.F. Toney, J. Huang, Z. Bao, Ultra-high mobility transparent organic thin film transistors grown by an off-centre spin-coating method, Nat. Commun. 5 (2014) 3005.

[56] M. Yang, Y. Zhou, Y. Zeng, C.-S. Jiang, N.P. Padture, K. Zhu, Square-centimeter solution-processed planar $CH_3NH_3PbI_3$ perovskite solar cells with efficiency exceeding 15%, Adv. Mater. 27 (2015) 6363–6370.

[57] B. Ding, Y. Li, S.-Y. Huang, Q.-Q. Chu, C.-X. Li, C.-J. Li, G.-J. Yang, Material nucleation/growth competition tuning towards highly reproducible planar perovskite solar cells with efficiency exceeding 20%, J. Mater. Chem. A 5 (2017) 6840–6848.

[58] M. Yang, Z. Li, M.O. Reese, O.G. Reid, D.H. Kim, S. Siol, T.R. Klein, Y. Yan, J.J. Berry, M.F.A.M. van Hest, K. Zhu, Perovskite ink with wide processing window for scalable high-efficiency solar cells, Nat. Energy 2 (2017) 17038.

[59] Q. Jiang, L. Zhang, H. Wang, X. Yang, J. Meng, H. Liu, Z. Yin, J. Wu, X. Zhang, J. You, Enhanced electron extraction using SnO_2 for high-efficiency planar-structure $HC(NH_2)_2PbI_3$-based perovskite solar cells, Nat. Energy 2 (2016) 16177.

[60] S. Das, B. Yang, G. Gu, P.C. Joshi, I.N. Ivanov, C.M. Rouleau, T. Aytug, D.B. Geohegan, K. Xiao, High-performance flexible perovskite solar cells by using a combination of ultrasonic spray-coating and low thermal budget photonic curing, ACS Photonics 2 (2015) 680–686.

[61] S. Gamliel, A. Dymshits, S. Aharon, E. Terkieltaub, L. Etgar, Micrometer sized perovskite crystals in planar hole conductor free solar cells, J. Phys. Chem. C 119 (2015) 19722–19728.

[62] X. Xia, H. Li, W. Wu, Y. Li, D. Fei, C. Gao, X. Liu, Efficient light harvester layer prepared by solid/mist interface reaction for perovskite solar cells, ACS Appl. Mater. Interfaces 7 (2015) 16907–16912.

[63] C.F.J. Lau, X. Deng, Q. Ma, J. Zheng, J.S. Yun, M.A. Green, S. Huang, A.W.Y. Ho-Baillie, $CsPbIBr_2$ perovskite solar cell by spray-assisted deposition, ACS Energy Lett. 1 (2016) 573–577.

[64] X. Xia, W. Wu, H. Li, B. Zheng, Y. Xue, J. Xu, D. Zhang, C. Gao, X. Liu, Spray reaction prepared $FA_{1-x}Cs_xPbI_3$ solid solution as a light harvester for perovskite solar cells with improved humidity stability, RSC Adv. 6 (2016) 14792–14798.

[65] Y.-S. Jung, K. Hwang, F.H. Scholes, S.E. Watkins, D.-Y. Kim, D. Vak, Differentially pumped spray deposition as a rapid screening tool for organic and perovskite solar cells, Sci. Rep. 6 (2016) 20357.

[66] Z. Wang, Z. Shi, T. Li, Y. Chen, W. Huang, Stability of perovskite solar cells: a prospective on the substitution of the A cation and X anion, Angew. Chem. Int. Ed. 56 (2017) 1190–1212.

[67] M. Remeika, S.R. Raga, S. Zhang, Y.B. Qi, Transferrable optimization of spray-coated PbI_2 films for perovskite solar cell fabrication, J. Mater. Chem. A 5 (2017) 5709–5718.

[68] J.H. Heo, M.H. Lee, M.H. Jang, S.H. Im, Highly efficient $CH_3NH_3PbI_{3-x}Cl_x$ mixed halide perovskite solar cells prepared by re-dissolution and crystal grain growth via spray coating, J. Mater. Chem. A 4 (2016) 17636–17642.

[69] W. Nie, H. Tsai, R. Asadpour, J.C. Blancon, A.J. Neukirch, G. Gupta, J.J. Crochet, M. Chhowalla, S. Tretiak, M.A. Alam, H.L. Wang, A.D. Mohite, Solar cells. High-efficiency solution-processed perovskite solar cells with millimeter-scale grains, Science 347 (2015) 522–525.

[70] J.H. Kim, S.T. Williams, N. Cho, C.-C. Chueh, A.K.Y. Jen, Enhanced environmental stability of planar heterojunction perovskite solar cells based on blade-coating, Adv. Energy Mater. 5 (2015) 1401229.

[71] Z. Yang, C.-C. Chueh, F. Zuo, J.H. Kim, P.-W. Liang, A.K.Y. Jen, High-performance fully printable perovskite solar cells via blade-coating technique under the ambient condition, Adv. Energy Mater. 5 (2015) 1500328.

[72] H. Back, J. Kim, G. Kim, T. Kyun Kim, H. Kang, J. Kong, S. Ho Lee, K. Lee, Interfacial modification of hole transport layers for efficient large-area perovskite solar cells achieved via blade-coating, Sol. Energy Mater. Sol. Cells 144 (2016) 309–315.

[73] A.T. Mallajosyula, K. Fernando, S. Bhatt, A. Singh, B.W. Alphenaar, J.-C. Blancon, W. Nie, G. Gupta, A.D. Mohite, Large-area hysteresis-free perovskite solar cells via temperature controlled doctor blading under ambient environment, Appl. Mater. Today 3 (2016) 96–102.

[74] D. Vak, K. Hwang, A. Faulks, Y.-S. Jung, N. Clark, D.-Y. Kim, G.J. Wilson, S.E. Watkins, 3D printer based slot-die coater as a lab-to-fab translation tool for solution-processed solar cells, Adv. Energy Mater. 5 (2015) 1401539.

[75] G. Cotella, J. Baker, D. Worsley, F. De Rossi, C. Pleydell-Pearce, M. Carnie, T. Watson, One-step deposition by slot-die coating of mixed lead halide perovskite for photovoltaic applications, Sol. Energy Mater. Sol. Cells 159 (2017) 362–369.

[76] T. Qin, W. Huang, J.-E. Kim, D. Vak, C. Forsyth, C.R. McNeill, Y.-B. Cheng, Amorphous hole-transporting layer in slot-die coated perovskite solar cells, Nano Energy 31 (2017) 210–217.

[77] Z. Ku, Y. Rong, M. Xu, T. Liu, H. Han, Full printable processed mesoscopic $CH_3NH_3PbI_3/TiO_2$ heterojunction solar cells with carbon counter electrode, Sci. Rep. 3 (2013) 3132.

[78] A. Mei, X. Li, L. Liu, Z. Ku, T. Liu, Y. Rong, M. Xu, M. Hu, J. Chen, Y. Yang, M. Grätzel, H. Han, A hole-conductor–free, fully printable mesoscopic perovskite solar cell with high stability, Science 345 (2014) 295–298.

[79] X. Li, M. Tschumi, H. Han, S.S. Babkair, R.A. Alzubaydi, A.A. Ansari, S.S. Habib, M.K. Nazeeruddin, S.M. Zakeeruddin, M. Grätzel, Outdoor performance and stability under elevated temperatures and long-term light soaking of triple-layer mesoporous perovskite photovoltaics, Energy Technol. 3 (2015) 551–555.

[80] Z. Wei, H. Chen, K. Yan, S. Yang, Inkjet printing and instant chemical transformation of a $CH_3NH_3PbI_3$/nanocarbon electrode and interface for planar perovskite solar cells, Angew. Chem. Int. Ed. 126 (2014) 13455–13459.

[81] S.-G. Li, K.-J. Jiang, M.-J. Su, X.-P. Cui, J.-H. Huang, Q.-Q. Zhang, X.-Q. Zhou, L.-M. Yang, Y.-L. Song, Inkjet printing of $CH_3NH_3PbI_3$ on a mesoscopic TiO_2 film for highly efficient perovskite solar cells, J. Mater. Chem. A 3 (2015) 9092–9097.

[82] M. Liu, M.B. Johnston, H.J. Snaith, Efficient planar heterojunction perovskite solar cells by vapour deposition, Nature 501 (2013) 395–398.

[83] M.R. Leyden, L.K. Ono, S.R. Raga, Y. Kato, S. Wang, Y.B. Qi, High performance perovskite solar cells by hybrid chemical vapor deposition, J. Mater. Chem. A 2 (2014) 18742–18745.

[84] L. Calió, C. Momblona, L. Gil-Escrig, S. Kazim, M. Sessolo, Á. Sastre-Santos, H.J. Bolink, S. Ahmad, Vacuum deposited perovskite solar cells employing dopant-free triazatruxene as the hole transport material, Sol. Energy Mater. Sol. Cells 163 (2017) 237–241.

[85] C. Momblona, L. Gil-Escrig, E. Bandiello, E.M. Hutter, M. Sessolo, K. Lederer, J. Blochwitz-Nimoth, H.J. Bolink, Efficient vacuum deposited p-i-n and n-i-p perovskite solar cells employing doped charge transport layers, Energy Environ. Sci. 9 (2016) 3456–3463.

[86] S.R. Raga, Y.B. Qi, The effect of impurities on the impedance spectroscopy response of $CH_3NH_3PbI_3$ perovskite solar cells, J. Phys. Chem. C 120 (2016) 28519–28526.

[87] L. Qiu, L.K. Ono, Y. Jiang, M.R. Leyden, S.R. Raga, S. Wang, Y.B. Qi, Engineering interface structure to improve efficiency and stability of organometal halide perovskite solar cells, J. Phys. Chem. B (2017), http://dx.doi.org/10.1021/acs.jpcb.1027b03921.

[88] M.-C. Jung, Y.B. Qi, Dopant interdiffusion effects in n-i-p structured spiro-OMeTAD hole transport layer of organometal halide perovskite solar cells, Org. Electron. 31 (2016) 71–76.

[89] S.-Y. Hsiao, H.-L. Lin, W.-H. Lee, W.-L. Tsai, K.-M. Chiang, W.-Y. Liao, C.-Z. Ren-Wu, C.-Y. Chen, H.-W. Lin, Efficient all-vacuum deposited perovskite solar cells by controlling reagent partial pressure in high vacuum, Adv. Mater. 28 (2016) 7013–7019.

[90] H. Tan, A. Jain, O. Voznyy, X. Lan, F.P. García de Arquer, J.Z. Fan, R. Quintero-Bermudez, M. Yuan, B. Zhang, Y. Zhao, F. Fan, P. Li, L.N. Quan, Y. Zhao, Z.-H. Lu, Z. Yang, S. Hoogland, E.H. Sargent, Efficient and stable solution-processed planar perovskite solar cells via contact passivation, Science 355 (2017) 722–726.

[91] W. Chen, L. Xu, X. Feng, J. Jie, Z. He, Metal acetylacetonate series in interface engineering for full low-temperature-processed, high-performance, and stable planar perovskite solar cells with conversion efficiency over 16% on 1 cm^2 scale, Adv. Mater. 29 (2017) 1603923.

[92] L.-L. Gao, C.-X. Li, C.-J. Li, G.-J. Yang, Large-area high-efficiency perovskite solar cells based on perovskite films dried by the multi-flow air knife method in air, J. Mater. Chem. A 5 (2017) 1548–1557.

[93] Z. Yang, B. Cai, B. Zhou, T. Yao, W. Yu, S. Liu, W.-H. Zhang, C. Li, An up-scalable approach to $CH_3NH_3PbI_3$ compact films for high-performance perovskite solar cells, Nano Energy 15 (2015) 670–678.

[94] M. Park, J.-S. Park, I.K. Han, J.Y. Oh, High-performance flexible and air-stable perovskite solar cells with a large active area based on poly(3-hexylthiophene) nanofibrils, J. Mater. Chem. A 4 (2016) 11307–11316.

[95] H. Shen, Y. Wu, J. Peng, T. Duong, X. Fu, C. Barugkin, T.P. White, K. Weber, K.R. Catchpole, Improved reproducibility for perovskite solar cells with 1 cm^2 active area by a modified two-step process, ACS Appl. Mater. Interfaces 9 (2017) 5974–5981.

[96] F. Matteocci, L. Cinà, E. Lamanna, S. Cacovich, G. Divitini, P.A. Midgley, C. Ducati, A. Di Carlo, Encapsulation for long-term stability enhancement of perovskite solar cells, Nano Energy 30 (2016) 162–172.

[97] C.-H. Chiang, M.K. Nazeeruddin, M. Gratzel, C.-G. Wu, The synergistic effect of H_2O and DMF towards stable and 20% efficiency inverted perovskite solar cells, Energy Environ. Sci. 10 (2017) 808–817.

[98] X. Chen, H. Cao, H. Yu, H. Zhu, H. Zhou, L. Yang, S. Yin, Large-area, high-quality organic-inorganic hybrid perovskite thin films via a controlled vapor-solid reaction, J. Mater. Chem. A 4 (2016) 9124–9132.

[99] F. Matteocci, S. Razza, F. Di Giacomo, S. Casaluci, G. Mincuzzi, T.M. Brown, A. D'Epifanio, S. Licoccia, A. Di Carlo, Solid-state solar modules based on mesoscopic organometal halide perovskite: a route towards the up-scaling process, Phys. Chem. Chem. Phys. 16 (2014) 3918–3923.

[100] F. Matteocci, L. Cinà, F. Di Giacomo, S. Razza, A.L. Palma, A. Guidobaldi, A. D'Epifanio, S. Licoccia, T.M. Brown, A. Reale, A. Di Carlo, High efficiency photovoltaic module based on mesoscopic organometal halide perovskite, Prog. Photovolt. Res. Appl. 24 (2016) 436–445.

[101] W. Qiu, T. Merckx, M. Jaysankar, C. Masse de la Huerta, L. Rakocevic, W. Zhang, U.W. Paetzold, R. Gehlhaar, L. Froyen, J. Poortmans, D. Cheyns,

H.J. Snaith, P. Heremans, Pinhole-free perovskite films for efficient solar modules, Energy Environ. Sci. 9 (2016) 484–489.
[102] A. Agresti, S. Pescetelli, A.L. Palma, A.E. Del Rio Castillo, D. Konios, G. Kakavelakis, S. Razza, L. Cinà, E. Kymakis, F. Bonaccorso, A. Di Carlo, Graphene interface engineering for perovskite solar modules: 12.6% power conversion efficiency over 50 cm^2 active area, ACS Energy Lett. 2 (2017) 279–287.
[103] J.H. Heo, H.J. Han, D. Kim, T.K. Ahn, S.H. Im, Hysteresis-less inverted $CH_3NH_3PbI_3$ planar perovskite hybrid solar cells with 18.1% power conversion efficiency, Energy Environ. Sci. 8 (2015) 1602–1608.
[104] D. Yang, Z. Yang, W. Qin, Y.L. Zhang, S.Z. Liu, C. Li, Alternating precursor layer deposition for highly stable perovskite films towards efficient solar cells using vacuum deposition, J. Mater. Chem. A 3 (2015) 9401–9405.
[105] O. Malinkiewicz, A. Yella, Y.H. Lee, G.M. Espallargas, M. Graetzel, M.K. Nazeeruddin, H.J. Bolink, Perovskite solar cells employing organic charge-transport layers, Nat. Photonics 8 (2014) 128–132.
[106] M.R. Leyden, M.V. Lee, S.R. Raga, Y.B. Qi, Large formamidinium lead trihalide perovskite solar cells using chemical vapor deposition with high reproducibility and tunable chlorine concentrations, J. Mater. Chem. A 3 (2015) 16097–16103.
[107] P.-S. Shen, J.-S. Chen, Y.-H. Chiang, M.-H. Li, T.-F. Guo, P. Chen, Low-pressure hybrid chemical vapor growth for efficient perovskite solar cells and large-area module, Adv. Mater. Interfaces 3 (2016) 1500849.
[108] G. Niu, X. Guo, L. Wang, Review of recent progress in chemical stability of perovskite solar cells, J. Mater. Chem. A 3 (2015) 8970–8980.
[109] T.A. Berhe, W.-N. Su, C.-H. Chen, C.-J. Pan, J.-H. Cheng, H.-M. Chen, M.-C. Tsai, L.-Y. Chen, A.A. Dubale, B.-J. Hwang, Organometal halide perovskite solar cells: degradation and stability, Energy Environ. Sci. 9 (2016) 323–356.
[110] E.J. Juarez-Perez, Z. Hawash, S.R. Raga, L.K. Ono, Y.B. Qi, Thermal degradation of $CH_3NH_3PbI_3$ perovskite into NH_3 and CH_3I gases observed by coupled thermogravimetry-mass spectrometry analysis, Energy Environ. Sci. 9 (2016) 3406–3410.
[111] S. Wang, Y. Jiang, Emilio J. Juarez-Perez, Luis K. Ono, Y.B. Qi, Accelerated degradation of methylammonium lead iodide perovskites induced by exposure to iodine vapour, Nat. Energy 2 (2016) 16195.
[112] J. Yang, B.D. Siempelkamp, E. Mosconi, F. De Angelis, T.L. Kelly, Origin of the thermal instability in $CH_3NH_3PbI_3$ thin films deposited on ZnO, Chem. Mater. 27 (2015) 4229–4236.
[113] Y. Dkhissi, S. Meyer, D. Chen, H.C. Weerasinghe, L. Spiccia, Y.-B. Cheng, R.A. Caruso, Stability comparison of perovskite solar cells based on zinc oxide and titania on polymer substrates, ChemSusChem 9 (2016) 687–695.
[114] T. Leijtens, G.E. Eperon, S. Pathak, A. Abate, M.M. Lee, H.J. Snaith, Overcoming ultraviolet light instability of sensitized TiO_2 with meso-superstructured organometal tri-halide perovskite solar cells, Nat. Commun. 4 (2013) 2885.
[115] N. Ahn, K. Kwak, M.S. Jang, H. Yoon, B.Y. Lee, J.-K. Lee, P.V. Pikhitsa, J. Byun, M. Choi, Trapped charge-driven degradation of perovskite solar cells, Nat. Commun. 7 (2016) 13422.
[116] Z. Hawash, L.K. Ono, S.R. Raga, M.V. Lee, Y.B. Qi, Air-exposure induced dopant redistribution and energy level shifts in spin-coated spiro-MeOTAD films, Chem. Mater. 27 (2015) 562–569.
[117] L.K. Ono, S.R. Raga, M. Remeika, A.J. Winchester, A. Gabe, Y.B. Qi, Pinhole-free hole transport layers significantly improve the stability of $MAPbI_3$-based perovskite solar cells under operating conditions, J. Mater. Chem. A 3 (2015) 15451–15456.
[118] M.-C. Jung, S.R. Raga, L.K. Ono, Y.B. Qi, Substantial improvement of perovskite solar cells stability by pinhole-free hole transport layer with doping engineering, Sci. Rep. 5 (2015) 9863.
[119] E.J. Juarez-Perez, M.R. Leyden, S. Wang, L.K. Ono, Z. Hawash, Y.B. Qi, Role of the dopants on the morphological and transport properties of spiro-MeOTAD hole transport layer, Chem. Mater. 28 (2016) 5702–5709.
[120] S. Wang, M. Sina, P. Parikh, T. Uekert, B. Shahbazian, A. Devaraj, Y.S. Meng, Role of 4-tert-Butylpyridine as a hole transport layer morphological controller in perovskite solar cells, Nano Lett. 16 (2016) 5594–5600.
[121] W. Li, H. Dong, L. Wang, N. Li, X. Guo, J. Li, Y. Qiu, Montmorillonite as bifunctional buffer layer material for hybrid perovskite solar cells with protection from corrosion and retarding recombination, J. Mater. Chem. A 2 (2014) 13587–13592.
[122] Z. Hawash, L.K. Ono, Y.B. Qi, Recent advances in spiro-MeOTAD hole transport material and its applications in organic-inorganic halide perovskite solar cells, Adv. Mater. Interfaces 4 (2017), 1700623.
[123] K. Domanski, J.-P. Correa-Baena, N. Mine, M.K. Nazeeruddin, A. Abate, M. Saliba, W. Tress, A. Hagfeldt, M. Grätzel, Not all that glitters is gold: metal-migration-induced degradation in perovskite solar cells, ACS Nano 10 (2016) 6306–6314.
[124] Y. Kato, L.K. Ono, M.V. Lee, S. Wang, S.R. Raga, Y.B. Qi, Silver iodide formation in methyl ammonium lead iodide perovskite solar cells with silver top electrodes, Adv. Mater. Interfaces 2 (2015) 1500195.
[125] Y. Han, S. Meyer, Y. Dkhissi, K. Weber, J.M. Pringle, U. Bach, L. Spiccia, Y.-B. Cheng, Degradation observations of encapsulated planar $CH_3NH_3PbI_3$ perovskite solar cells at high temperatures and humidity, J. Mater. Chem. A 3 (2015) 8139–8147.
[126] H.-S. Kim, J.-Y. Seo, N.-G. Park, Material and device stability in perovskite solar cells, ChemSusChem 9 (2016) 2528–2540.
[127] I.C. Smith, E.T. Hoke, D. Solis-Ibarra, M.D. McGehee, H.I. Karunadasa, A layered hybrid perovskite solar-cell absorber with enhanced moisture stability, Angew. Chem. Int. Ed. 126 (2014) 11414–11417.
[128] D.H. Cao, C.C. Stoumpos, O.K. Farha, J.T. Hupp, M.G. Kanatzidis, 2D homologous perovskites as light-absorbing materials for solar cell applications, J. Am. Chem. Soc. 137 (2015) 7843–7850.
[129] Z. Wang, Q. Lin, F.P. Chmiel, N. Sakai, L.M. Herz, H.J. Snaith, Efficient ambient-air-stable solar cells with 2D–3D heterostructured butylammonium-caesium-formamidinium lead halide perovskites, Nat. Energy 6 (2017) 17135.
[130] G. Grancini, C. Roldán-Carmona, I. Zimmermann, E. Mosconi, X. Lee, D. Martineau, S. Narbey, F. Oswald, F. De Angelis, M. Graetzel, M.K. Nazeeruddin, One-year stable perovskite solar cells by 2D/3D interface engineering, Nat. Commun. 8 (2017) 15684.
[131] H. Chen, S. Yang, Carbon-based perovskite solar cells without hole transport materials: the front runner to the market? Adv. Mater. 29 (2017) 1603994.
[132] H. Zhang, H. Wang, S.T. Williams, D. Xiong, W. Zhang, C.-C. Chueh, W. Chen, A.K.Y. Jen, $SrCl_2$ derived perovskite facilitating a high efficiency of 16% in hole-conductor-free fully printable mesoscopic perovskite solar cells, Adv. Mater. 29 (2017) 1606608.
[133] A.M. Soufiani, Z. Hameiri, S. Meyer, S. Lim, M.J.Y. Tayebjee, J.S. Yun, A. Ho-Baillie, G.J. Conibeer, L. Spiccia, M.A. Green, Lessons learnt from spatially resolved electro- and photoluminescence imaging: interfacial delamination in $CH_3NH_3PbI_3$ planar perovskite solar cells upon illumination, Adv. Energy Mater. (2016) 1602111.
[134] B. Hailegnaw, S. Kirmayer, E. Edri, G. Hodes, D. Cahen, Rain on methylammonium lead iodide based perovskites: possible environmental effects of perovskite solar cells, J. Phys. Chem. Lett. 6 (2015) 1543–1547.
[135] Q. Dong, F. Liu, M.K. Wong, H.W. Tam, A.B. Djurišić, A. Ng, C. Surya, W.K. Chan, A.M.C. Ng, Encapsulation of perovskite solar cells for high humidity conditions, ChemSusChem 9 (2016) 2597–2603.
[136] T. Leijtens, G.E. Eperon, N.K. Noel, S.N. Habisreutinger, A. Petrozza, H.J. Snaith, Stability of metal halide perovskite solar cells, Adv. Energy Mater. 5 (2015) 1500963.
[137] K. Wojciechowski, T. Leijtens, S. Siprova, C. Schlueter, M.T. Hörantner, J.T.-W. Wang, C.-Z. Li, A.K.Y. Jen, T.-L. Lee, H.J. Snaith, C60 as an efficient n-type compact layer in perovskite solar cells, J. Phys. Chem. Lett. 6 (2015) 2399–2405.
[138] S.K. Pathak, A. Abate, P. Ruckdeschel, B. Roose, K.C. Gödel, Y. Vaynzof, A. Santhala, S.-I. Watanabe, D.J. Hollman, N. Noel, A. Sepe, U. Wiesner, R. Friend, H.J. Snaith, U. Steiner, Performance and stability enhancement of dye-sensitized and perovskite solar cells by Al doping of TiO_2, Adv. Func. Mater. 24 (2014) 6046–6055.
[139] S.K. Pathak, A. Abate, T. Leijtens, D.J. Hollman, J. Teuscher, L. Pazos, P. Docampo, U. Steiner, H.J. Snaith, Towards long-term photostability of solid-state dye sensitized solar cells, Adv. Energy Mater. 4 (2014) 1301667.
[140] F. Bella, G. Griffini, J.P. Correa-Baena, G. Saracco, M. Gratzel, A. Hagfeldt, S. Turri, C. Gerbaldi, Improving efficiency and stability of perovskite solar cells with photocurable fluoropolymers, Science 354 (2016) 203–206.
[141] S.G. Hashmi, A. Tiihonen, D. Martineau, M. Ozkan, P. Vivo, K. Kaunisto, V. Ulla, S.M. Zakeeruddin, M. Gratzel, Long term stability of air processed inkjet infiltrated carbon-based printed perovskite solar cells under intense ultraviolet light soaking, J. Mater. Chem. A 5 (2017) 4797–4802.
[142] S.-W. Lee, S. Kim, S. Bae, K. Cho, T. Chung, L.E. Mundt, S. Lee, S. Park, H. Park, M.C. Schubert, S.W. Glunz, Y. Ko, Y. Jun, Y. Kang, H.-S. Lee, D. Kim, UV degradation and recovery of perovskite solar cells, Sci. Rep. 6 (2016) 38150.
[143] S.S. Shin, E.J. Yeom, W.S. Yang, S. Hur, M.G. Kim, J. Im, J. Seo, J.H. Noh, S.I. Seok, Colloidally prepared La-doped $BaSnO_3$ electrodes for efficient, photostable perovskite solar cells, Science 356 (2017) 167–171.
[144] M. Saliba, T. Matsui, K. Domanski, J.Y. Seo, A. Ummadisingu, S.M. Zakeeruddin, J.P. Correa-Baena, W.R. Tress, A. Abate, A. Hagfeldt, M. Gratzel, Incorporation of rubidium cations into perovskite solar cells improves photovoltaic performance, Science 354 (2016) 206–209.
[145] K.A. Bush, A.F. Palmstrom, Z.J. Yu, M. Boccard, R. Cheacharoen, J.P. Mailoa, D.P. McMeekin, R.L.Z. Hoye, C.D. Bailie, T. Leijtens, I.M. Peters, M.C. Minichetti, N. Rolston, R. Prasanna, S. Sofia, D. Harwood, W. Ma, F. Moghadam, H.J. Snaith, T. Buonassisi, Z.C. Holman, S.F. Bent, M.D. McGehee, 23.6%-efficient monolithic perovskite/silicon tandem solar cells with improved stability, Nat. Energy 2 (2017) 17009.
[146] F. Huang, L. Jiang, A.R. Pascoe, Y. Yan, U. Bach, L. Spiccia, Y.-B. Cheng, Fatigue behavior of planar $CH_3NH_3PbI_3$ perovskite solar cells revealed by light on/off diurnal cycling, Nano Energy 27 (2016) 509–514.
[147] E.H. Anaraki, A. Kermanpur, L. Steier, K. Domanski, T. Matsui, W. Tress, M. Saliba, A. Abate, M. Gratzel, A. Hagfeldt, J.-P. Correa-Baena, Highly efficient and stable planar perovskite solar cells by solution-processed tin oxide, Energy Environ. Sci. 9 (2016) 3128–3134.
[148] M.O. Reese, S.A. Gevorgyan, M. Jørgensen, E. Bundgaard, S.R. Kurtz, D.S. Ginley, D.C. Olson, M.T. Lloyd, P. Morvillo, E.A. Katz, A. Elschner, O. Haillant, T.R. Currier, V. Shrotriya, M. Hermenau, M. Riede, K.R. Kirov, G. Trimmel, T. Rath, O. Inganäs, F. Zhang, M. Andersson, K. Tvingstedt, M. Lira-Cantu, D. Laird, C. McGuiness, S. Gowrisanker, M. Pannone, M. Xiao, J. Hauch, R. Steim, D.M. DeLongchamp, R. Rösch, H. Hoppe, N. Espinosa, A. Urbina, G. Yaman-Uzunoglu, J.-B. Bonekamp, A.J.J.M. van Breemen, C. Girotto, E. Voroshazi, F.C. Krebs, Consensus stability testing protocols for organic photovoltaic materials and devices, Sol. Energy Mater. Sol. Cells 95 (2011) 1253–1267.
[149] K. Aitola, K. Domanski, J.P. Correa-Baena, K. Sveinbjornsson, M. Saliba, A. Abate, M. Gratzel, E. Kauppinen, E.M.J. Johansson, W. Tress, A. Hagfeldt,

G. Boschloo, High temperature-stable perovskite solar cell based on low-cost carbon nanotube hole contact, Adv. Mater. 29 (2017) 1606398.
[150] F. Zhang, W. Shi, J. Luo, N. Pellet, C. Yi, X. Li, X. Zhao, T.J.S. Dennis, X. Li, S. Wang, Y. Xiao, S.M. Zakeeruddin, D. Bi, M. Gratzel, Isomer-pure bis-PCBM-assisted crystal engineering of perovskite solar cells showing excellent efficiency and stability, Adv. Mater. 29 (2017) 1606806.
[151] S. Schuller, P. Schilinsky, J. Hauch, C.J. Brabec, Determination of the degradation constant of bulk heterojunction solar cells by accelerated lifetime measurements, Appl. Phys. A Mater. 79 (2004) 37–40.
[152] H. Zhou, Y. Shi, Q. Dong, H. Zhang, Y. Xing, K. Wang, Y. Du, T. Ma, Hole-conductor-free, metal-electrode-free $TiO_2/CH_3NH_3PbI_3$ heterojunction solar cells based on a low-temperature carbon electrode, J. Phys. Chem. Lett. 5 (2014) 3241–3246.
[153] S.S. Mali, C.S. Shim, C.K. Hong, Highly stable and efficient solid-state solar cells based on methylammonium lead bromide ($CH_3NH_3PbBr_3$) perovskite quantum dots, NPG Asia Mater. 7 (2015) e208.
[154] Y.S. Kwon, J. Lim, H.-J. Yun, Y.-H. Kim, T. Park, A diketopyrrolopyrrole-containing hole transporting conjugated polymer for use in efficient stable organic-inorganic hybrid solar cells based on a perovskite, Energy Environ. Sci. 7 (2014) 1454–1460.
[155] D. Bi, W. Tress, M.I. Dar, P. Gao, J. Luo, C. Renevier, K. Schenk, A. Abate, F. Giordano, J.P. Correa Baena, J.D. Decoppet, S.M. Zakeeruddin, M.K. Nazeeruddin, M. Gratzel, A. Hagfeldt, Efficient luminescent solar cells based on tailored mixed-cation perovskites, Sci. Adv. 2 (2016) e1501170.
[156] H.C. Weerasinghe, Y. Dkhissi, A.D. Scully, R.A. Caruso, Y.-B. Cheng, Encapsulation for improving the lifetime of flexible perovskite solar cells, Nano Energy 18 (2015) 118–125.
[157] J.P. Correa Baena, L. Steier, W. Tress, M. Saliba, S. Neutzner, T. Matsui, F. Giordano, T.J. Jacobsson, A.R. Srimath Kandada, S.M. Zakeeruddin, A. Petrozza, A. Abate, M.K. Nazeeruddin, M. Gratzel, A. Hagfeldt, Highly efficient planar perovskite solar cells through band alignment engineering, Energy Environ. Sci. 8 (2015) 2928–2934.
[158] Y. Li, Y. Zhao, Q. Chen, Y. Yang, Y. Liu, Z. Hong, Z. Liu, Y.-T. Hsieh, L. Meng, Y. Li, Y. Yang, Multifunctional fullerene derivative for interface engineering in perovskite solar cells, J. Am. Chem. Soc. 137 (2015) 15540–15547.
[159] J. You, L. Meng, T.-B. Song, T.-F. Guo, Y. Yang, W.-H. Chang, Z. Hong, H. Chen, H. Zhou, Q. Chen, Y. Liu, N. De Marco, Y. Yang, Improved air stability of perovskite solar cells via solution-processed metal oxide transport layers, Nat. Nano 11 (2016) 75–81.
[160] C.-Y. Chang, K.-T. Lee, W.-K. Huang, H.-Y. Siao, Y.-C. Chang, High-performance, air-stable, low-temperature processed semitransparent perovskite solar cells enabled by atomic layer deposition, Chem. Mater. 27 (2015) 5122–5130.
[161] Y. Rong, X. Hou, Y. Hu, A. Mei, L. Liu, P. Wang, H. Han, Synergy of ammonium chloride and moisture on perovskite crystallization for efficient printable mesoscopic solar cells, Nat. Commun. 8 (2017) 14555.
[162] J. Zhao, X. Zheng, Y. Deng, T. Li, Y. Shao, A. Gruverman, J. Shield, J. Huang, Is Cu a stable electrode material in hybrid perovskite solar cells for a 30-year lifetime? Energy Environ. Sci. 9 (2016) 3650–3656.
[163] Z. Wang, D.P. McMeekin, N. Sakai, S. van Reenen, K. Wojciechowski, J.B. Patel, M.B. Johnston, H.J. Snaith, Efficient and air-stable mixed-cation lead mixed-halide perovskite solar cells with n-doped organic electron extraction layers, Adv. Mater. 29 (2017) 1604186.
[164] A.J. Davidson, S.P. Binks, J. Gediga, Lead industry life cycle studies: environmental impact and life cycle assessment of lead battery and architectural sheet production, Int. J. Life Cycle Assess. 21 (2016) 1624–1636.
[165] J.M. Kadro, N. Pellet, F. Giordano, A. Ulianov, O. Muntener, J. Maier, M. Gratzel, A. Hagfeldt, Proof-of-concept for facile perovskite solar cell recycling, Energy Environ. Sci. 9 (2016) 3172–3179.
[166] D. Bryant, P. Greenwood, J. Troughton, M. Wijdekop, M. Carnie, M. Davies, K. Wojciechowski, H.J. Snaith, T. Watson, D. Worsley, A transparent conductive adhesive Laminate electrode for high-efficiency organic-inorganic lead halide perovskite solar cells, Adv. Mater. 26 (2014) 7499–7504.
[167] F. Guo, H. Azimi, Y. Hou, T. Przybilla, M. Hu, C. Bronnbauer, S. Langner, E. Spiecker, K. Forberich, C.J. Brabec, High-performance semitransparent perovskite solar cells with solution-processed silver nanowires as top electrodes, Nanoscale 7 (2015) 1642–1649.
[168] H. Sun, J. Deng, L. Qiu, X. Fang, H. Peng, Recent progress in solar cells based on one-dimensional nanomaterials, Energy Environ. Sci. 8 (2015) 1139–1159.
[169] A. Babayigit, A. Ethirajan, M. Muller, B. Conings, Toxicity of organometal halide perovskite solar cells, Nat. Mater. 15 (2016) 247–251.
[170] A. Babayigit, D. Duy Thanh, A. Ethirajan, J. Manca, M. Muller, H.-G. Boyen, B. Conings, Assessing the toxicity of Pb- and Sn-based perovskite solar cells in model organism Danio rerio, Sci. Rep. 6 (2016) 18721.
[171] T. Vorvolakos, S. Arseniou, M. Samakouri, There is no safe threshold for lead exposure: a literature review, Psychiatriki 27 (2016) 204–214.
[172] J. Calderone, and S. Gould, Here's how lead is poisoning American children, http://www.businessinsider.com/lead-health-child-flint-michigan-body-pollution-water-2016-2013 (Accessed 30 December 2016).
[173] G. Flora, D. Gupta, A. Tiwari, Toxicity of lead: a review with recent updates, Interdiscip. Toxicol. 5 (2012) 47–58.
[174] S. Chandrasekar, L. Lomasney, N. Derhammer, Systemic lead toxicity, Orthopedics 38 (2015) 592, 644–647.
[175] H. Delile, J. Blichert-Toft, J.-P. Goiran, S. Keay, F. Albarède, Lead in ancient Rome's city waters, Proc. Natl. Acad. Sci. 111 (2014) 6594–6599.
[176] H. Needleman, Lead poisoning, Ann. Rev. Med. 55 (2004) 209–222.
[177] L. Järup, Hazards of heavy metal contamination, Br. Med. Bull. 68 (2003) 167–182.
[178] S. Hernberg, Lead poisoning in a historical perspective, Am. J. Ind. Med. 38 (2000) 244–254.
[179] O.A. Ogunseitan, Power failure: the battered Legacy of leaded batteries, Environ. Sci. Technol. 50 (2016) 8401–8402.
[180] P. Gottesfeld, A.K. Pokhrel, Review: lead exposure in battery manufacturing and recycling in developing countries and among children in nearby communities, J. Occup. Environ. Hyg. 8 (2011) 520–532.
[181] W. Zhang, J. Yang, X. Wu, Y. Hu, W. Yu, J. Wang, J. Dong, M. Li, S. Liang, J. Hu, R.V. Kumar, A critical review on secondary lead recycling technology and its prospect, Renew. Sustain. Energy Rev. 61 (2016) 108–122.
[182] T. Fujimori, A. Eguchi, T. Agusa, N.M. Tue, G. Suzuki, S. Takahashi, P.H. Viet, S. Tanabe, H. Takigami, Lead contamination in surface soil on roads from used lead–acid battery recycling in Dong Mai, Northern Vietnam, J. Mater. Cycles Waste Manag. 18 (2016) 599–607.
[183] T.J. van der Kuijp, L. Huang, C.R. Cherry, Health hazards of China's lead-acid battery industry: a review of its market drivers, production processes, and health impacts, Environ. Health 12 (2013) 61.
[184] L.A. Frolova, D.V. Anokhin, K.L. Gerasimov, N.N. Dremova, P.A. Troshin, Exploring the effects of the Pb^{2+} substitution in $MAPbI_3$ on the photovoltaic performance of the hybrid perovskite solar cells, J. Phys. Chem. Lett. 7 (2016) 4353–4357.
[185] M.T. Klug, A. Osherov, A.A. Haghighirad, S.D. Stranks, P.R. Brown, S. Bai, J.T.W. Wang, X.N. Dang, V. Bulovic, H.J. Snaith, A.M. Belcher, Tailoring metal halide perovskites through metal substitution: influence on photovoltaic and material properties, Energy Environ. Sci. 10 (2017) 236–246.
[186] J. Zhang, M.-H. Shang, P. Wang, X. Huang, J. Xu, Z. Hu, Y. Zhu, L. Han, n-Type doping and energy states tuning in $CH_3NH_3Pb_{1-x}sb_{2x/3}I_3$ perovskite solar cells, ACS Energy Lett. 1 (2016) 535–541.
[187] J. Navas, A. Sanchez-Coronilla, J.J. Gallardo, N. Cruz Hernandez, J.C. Pinero, R. Alcantara, C. Fernandez-Lorenzo, D.M. De los Santos, T. Aguilar, J. Martin-Calleja, New insights into organic-inorganic hybrid perovskite $CH_3NH_3PbI_3$ nanoparticles. An experimental and theoretical study of doping in Pb^{2+} sites with Sn^{2+}, Sr^{2+}, Cd^{2+} and Ca^{2+}, Nanoscale 7 (2015) 6216–6229.
[188] P. Singh, P.J.S. Rana, P. Dhingra, P. Kar, Towards toxicity removal in lead based perovskite solar cells by compositional gradient using manganese chloride, J. Mater. Chem. C 4 (2016) 3101–3105.
[189] J.T.-W. Wang, Z. Wang, S. Pathak, W. Zhang, D.W. deQuilettes, F. Wisniveshy-Rocca-Rivarola, J. Huang, P.K. Nayak, J.B. Patel, H.A. Mohd Yusof, Y. Vaynzof, R. Zhu, I. Ramirez, J. Zhang, C. Ducati, C. Grovenor, M.B. Johnston, D.S. Ginger, R.J. Nicholas, H.J. Snaith, Efficient perovskite solar cells by metal ion doping, Energy Environ. Sci. 9 (2016) 2892–2901.
[190] R.L.Z. Hoye, R.E. Brandt, A. Osherov, V. Stevanović, S.D. Stranks, M.W.B. Wilson, H. Kim, A.J. Akey, J.D. Perkins, R.C. Kurchin, J.R. Poindexter, E.N. Wang, M.G. Bawendi, V. Bulović, T. Buonassisi, Methylammonium bismuth iodide as a lead-free, stable hybrid organic–inorganic solar absorber, Chem. Eur. J. 22 (2016) 2605–2610.
[191] A.L. Abdelhady, M.I. Saidaminov, B. Murali, V. Adinolfi, O. Voznyy, K. Katsiev, E. Alarousu, R. Comin, I. Dursun, L. Sinatra, E.H. Sargent, O.F. Mohammed, O.M. Bakr, Heterovalent dopant incorporation for bandgap and type engineering of perovskite crystals, J. Phys. Chem. Lett. 7 (2016) 295–301.
[192] Z.-K. Wang, M. Li, Y.-G. Yang, Y. Hu, H. Ma, X.-Y. Gao, L.-S. Liao, High efficiency Pb–In binary metal perovskite solar cells, Adv. Mater. 28 (2016) 6695–6703.
[193] W.A. Dunlap-Shohl, R. Younts, B.R. Gautam, K. Gundogdu, D.B. Mitzi, Effects of Cd diffusion and doping in high-performance perovskite solar cells using CdS as electron transport layer, J. Phys. Chem. C 120 (2016) 16437–16445.
[194] Q. Wang, Y. Shao, H. Xie, L. Lyu, X. Liu, Y. Gao, J. Huang, Qualifying composition dependent p and n self-doping in $CH_3NH_3PbI_3$, Appl. Phys. Lett. 105 (2014) 163508.
[195] D. Song, D. Wei, P. Cui, M. Li, Z. Duan, T. Wang, J. Ji, Y. Li, J.M. Mbengue, Y. Li, Y. He, M. Trevor, N.-G. Park, Dual function interfacial layer for highly efficient and stable lead halide perovskite solar cells, J. Mater. Chem. A 4 (2016) 6091–6097.
[196] D. Song, P. Cui, T. Wang, D. Wei, M. Li, F. Cao, X. Yue, P. Fu, Y. Li, Y. He, B. Jiang, M. Trevor, Managing carrier lifetime and doping property of lead halide perovskite by postannealing processes for highly efficient perovskite solar cells, J. Phys. Chem. C 119 (2015) 22812–22819.
[197] M.R. Filip, G.E. Eperon, H.J. Snaith, F. Giustino, Steric engineering of metal-halide perovskites with tunable optical band gaps, Nat. Commun. 5 (2014) 5757.
[198] Q. Chen, N. De Marco, Y. Yang, T.B. Song, C.C. Chen, H.X. Zhao, Z.R. Hong, H.P. Zhou, Y. Yang, Under the spotlight: the organic-inorganic hybrid halide perovskite for optoelectronic applications, Nano Today 10 (2015) 355–396.
[199] G. Kieslich, S. Sun, A.K. Cheetham, An extended Tolerance Factor approach for organic-inorganic perovskites, Chem. Sci. 6 (2015) 3430–3433.
[200] W. Travis, E.N.K. Glover, H. Bronstein, D.O. Scanlon, R.G. Palgrave, On the application of the tolerance factor to inorganic and hybrid halide perovskites: a revised system, Chem. Sci. 7 (2016) 4548–4556.
[201] M.R. Filip, F. Giustino, Computational screening of homovalent lead substitution in organic–inorganic halide perovskites, J. Phys. Chem. C 120 (2016) 166–173.
[202] S. Korbel, M.A.L. Marques, S. Botti, Stability and electronic properties of new inorganic perovskites from high-throughput ab initio calculations, J. Mater. Chem. C 4 (2016) 3157–3167.

[203] C. Zhang, L. Gao, S. Hayase, T. Ma, Current advancements in material research and techniques focusing on lead-free perovskite solar cells, Chem. Lett. 46 (2017) 1276–1284.
[204] N.J. Jeon, J.H. Noh, W.S. Yang, Y.C. Kim, S. Ryu, J. Seo, S.I. Seok, Compositional engineering of perovskite materials for high-performance solar cells, Nature 517 (2015) 476–480.
[205] Y. Zhou, Z. Zhou, M. Chen, Y. Zong, J. Huang, S. Pang, N.P. Padture, Doping and alloying for improved perovskite solar cells, J. Mater. Chem. A 4 (2016) 17623–17635.
[206] L.K. Ono, E.J. Juárez-Pérez, Y.B. Qi, Progress on novel perovskite materials and solar cells with mixed cations and halide anions, ACS Appl. Mater. Interfaces (2017), http://dx.doi.org/10.1021/acsami.1027b06001.
[207] F. Giustino, H.J. Snaith, Toward lead-free perovskite solar cells, ACS Energy Lett. 1 (2016) 1233–1240.
[208] Z.W. Xiao, W.W. Meng, J.B. Wang, D.B. Mitzi, Y.F. Yan, Searching for promising new perovskite-based photovoltaic absorbers: the importance of electronic dimensionality, Mater. Horiz. 4 (2017) 206–216.
[209] B.-W. Park, B. Philippe, X. Zhang, H. Rensmo, G. Boschloo, E.M.J. Johansson, Bismuth based hybrid perovskites $A_3Bi_2I_9$ (a: methylammonium or cesium) for solar cell application, Adv. Mater. 27 (2015) 6806–6813.
[210] M.B. Johansson, H. Zhu, E.M.J. Johansson, Extended photo-conversion spectrum in low-toxic bismuth halide perovskite solar cells, J. Phys. Chem. Lett. 7 (2016) 3467–3471.
[211] B. Saparov, J.-P. Sun, W. Meng, Z. Xiao, H.-S. Duan, O. Gunawan, D. Shin, I.G. Hill, Y. Yan, D.B. Mitzi, Thin-film deposition and characterization of a Sn-deficient perovskite derivative Cs_2SnI_6, Chem. Mater. 28 (2016) 2315–2322.
[212] B. Lee, C.C. Stoumpos, N. Zhou, F. Hao, C. Malliakas, C.-Y. Yeh, T.J. Marks, M.G. Kanatzidis, R.P.H. Chang, Air-stable molecular semiconducting iodosalts for solar cell applications: Cs_2SnI_6 as a hole conductor, J. Am. Chem. Soc. 136 (2014) 15379–15385.
[213] A.H. Slavney, T. Hu, A.M. Lindenberg, H.I. Karunadasa, A bismuth-halide double perovskite with long carrier recombination lifetime for photovoltaic applications, J. Am. Chem. Soc. 138 (2016) 2138–2141.
[214] E.T. McClure, M.R. Ball, W. Windl, P.M. Woodward, Cs_2AgBiX_6 (X = Br, Cl) new visible light absorbing, lead-free halide perovskite semiconductors, Chem. Mater. 28 (2016) 1348–1354.
[215] F. Wei, Z. Deng, S. Sun, F. Xie, G. Kieslich, D.M. Evans, M.A. Carpenter, P.D. Bristowe, A.K. Cheetham, The synthesis, structure and electronic properties of a lead-free hybrid inorganic-organic double perovskite $(MA)_2KBiCl_6$ (MA = methylammonium), Mater. Horiz. 3 (2016) 328–332.
[216] G. Volonakis, M.R. Filip, A.A. Haghighirad, N. Sakai, B. Wenger, H.J. Snaith, F. Giustino, Lead-free halide double perovskites via heterovalent substitution of noble metals, J. Phys. Chem. Lett. 7 (2016) 1254–1259.
[217] A.H. Slavney, R.W. Smaha, I.C. Smith, A. Jaffe, D. Umeyama, H.I. Karunadasa, Chemical approaches to addressing the instability and toxicity of lead-halide perovskite absorbers, Inorg. Chem. 56 (2017) 46–55.
[218] B. Saparov, D.B. Mitzi, Organic–inorganic perovskites: structural versatility for functional materials design, Chem. Rev. 116 (2016) 4558–4596.
[219] T. Singh, A. Kulkarni, M. Ikegami, T. Miyasaka, Effect of electron transporting layer on bismuth-based lead-free perovskite $(CH_3NH_3)_3$ Bi_2I_9 for photovoltaic applications, ACS Appl. Mater. Interfaces 8 (2016) 14542–14547.
[220] P.C. Harikesh, H.K. Mulmudi, B. Ghosh, T.W. Goh, Y.T. Teng, K. Thirumal, M. Lockrey, K. Weber, T.M. Koh, S. Li, S. Mhaisalkar, N. Mathews, Rb as an alternative cation for templating inorganic lead-free perovskites for solution processed photovoltaics, Chem. Mater. 28 (2016) 7496–7504.
[221] Y.-Y. Sun, J. Shi, J. Lian, W. Gao, M.L. Agiorgousis, P. Zhang, S. Zhang, Discovering lead-free perovskite solar materials with a split-anion approach, Nanoscale 8 (2016) 6284–6289.
[222] D. Cortecchia, H.A. Dewi, J. Yin, A. Bruno, S. Chen, T. Baikie, P.P. Boix, M. Grätzel, S. Mhaisalkar, C. Soci, N. Mathews, Lead-free $MA_2CuCl_xBr_{4-x}$ hybrid perovskites, Inorg. Chem. 55 (2016) 1044–1052.
[223] F. Hong, B. Saparov, W. Meng, Z. Xiao, D.B. Mitzi, Y. Yan, Viability of lead-free perovskites with mixed chalcogen and halogen anions for photovoltaic applications, J. Phys. Chem. C 120 (2016) 6435–6441.
[224] S. Vasala, M. Karppinen, $A_2B'B''O_6$ perovskites: a review, Prog. Solid State Chem. 43 (2015) 1–36.
[225] C.N. Savory, A. Walsh, D.O. Scanlon, Can Pb-Free halide double perovskites support high-efficiency solar cells? ACS Energy Lett. 1 (2016) 949–955.
[226] A. Kaltzoglou, M. Antoniadou, A.G. Kontos, C.C. Stoumpos, D. Perganti, E. Siranidi, V. Raptis, K. Trohidou, V. Psycharis, M.G. Kanatzidis, P. Falaras, Optical-vibrational properties of the Cs_2SnX_6 (X = Cl, Br, I) defect perovskites and hole-transport efficiency in dye-sensitized solar cells, J. Phys. Chem. C 120 (2016) 11777–11785.
[227] National Renewable Energy Laboratory (NREL). Research Cell Efficiency Records, http://www.nrel.gov/ncpv/images/efficiency_chart.jpg (Last date Accessed 21 March 2017).
[228] W. Shockley, H.J. Queisser, Detailed balance limit of efficiency of p-n junction solar cells, J. Appl. Phys. 32 (1961) 510–519.
[229] K.-F. Lin, S.H. Chang, K.-H. Wang, H.-M. Cheng, K.Y. Chiu, K.-M. Lee, S.-H. Chen, C.-G. Wu, Unraveling the high performance of tri-iodide perovskite absorber based photovoltaics with a non-polar solvent washing treatment, Sol. Energy Mater. Sol. Cells 141 (2015) 309–314.
[230] S. Razza, S. Castro-Hermosa, A.D. Carlo, T.M. Brown, Research update: large-area deposition, coating, printing, and processing techniques for the upscaling of perovskite solar cell technology, APL Mater. 4 (2016) 091508.
[231] B. Cai, Y. Xing, Z. Yang, W.-H. Zhang, J. Qiu, High performance hybrid solar cells sensitized by organolead halide perovskites, Energy Environ. Sci. 6 (2013) 1480–1485.
[232] R. F. Service, Perovskite solar cells gear up to go commercial, Science 354 (2016) 1214–1215.
[233] M.A. Green, A. Ho-Baillie, Perovskite solar cells: the birth of a new era in photovoltaics, ACS Energy Lett. 2 (2017) 822–830.
[234] M.A. Green, S.P. Bremner, Energy conversion approaches and materials for high-efficiency photovoltaics, Nat. Mater. 16 (2017) 23–34.
[235] C.R. Osterwald, T.J. McMahon, History of accelerated and qualification testing of terrestrial photovoltaic modules: a literature review, Prog. Photovolt. Res. Appl. 17 (2009) 11–33.
[236] B.J. Kim, D.H. Kim, S.L. Kwon, S.Y. Park, Z. Li, K. Zhu, H.S. Jung, Selective dissolution of halide perovskites as a step towards recycling solar cells, Nat. Commun. 7 (2016) 11735.
[237] N.K. Noel, S.N. Habisreutinger, B. Wenger, M.T. Klug, M.T. Horantner, M.B. Johnston, R.J. Nicholas, D.T. Moore, H.J. Snaith, A low viscosity, low boiling point, clean solvent system for the rapid crystallisation of highly specular perovskite films, Energy Environ. Sci. 10 (2017) 145–152.